Introduction

Based on work by Keith et al. (1997) at the Bingham and Tintic mining districts in Utah, evidence from the Bajo de la Alumbrera complex, and preliminary evidence from other porphyry systems, Halter et al. (2002a) proposed that the destabilization of magmatic sulfides and dissolution temperature of sulfide metals into magmatic ore fluids is responsible for producing the characteristic Au/Cu ratios shared by both the magmatic sulfides and the bulk ore body. This study compares the copper, silver and gold content and ratios of magmatic sulfide inclusions related to the Cu±Mo porphyry system of Yerington, Nevada, USA, and the high-sulfidation epithermal Au-Cu system of Yanacocha, Peru. These two groups of magmatic rocks are compared with one another to test whether or not the metal contents and ratios of magmatic sulfides in each large mining district dictate the average metal content and metal ratios of bulk ores. Samples of volcanic rocks spanning around 4 Ma from pre-ore to syn-ore in the Yanacocha district were chosen to determine the variation of sulfide mineralogy and metal content, and correlate these with mineralizing events.

Laser Ablation Inductively Coupled Plasma Mass Spectrometry (LA-ICPMS) and electron microprobe analysis were used to directly determine the metal contents of magmatic sulfide inclusions. A methodology for LA-ICPMS analysis of sulfides was developed for the OSU instrumentation, and included standardization, lab protocols, and estimation of detection limits of relevant trace metals.

Geologic Setting and Background Information

Where there is sufficient quantity of sulfide sulfur in a silicate melt, sulfide saturation may occur to produce immiscible sulfide and silicate liquids (Ebel and Naldrett, 1997). At lower temperatures, the sulfide melt crystallizes and may become sulfide minerals that may be trapped in the host silicate rock. The sizes of these sulfides vary greatly, from massive magmatic sulfide ore deposits to micrometer-sized blebs trapped in a silicate crystal. Regardless of the size of the sulfides, the properties remain similar. When there is a silicate melt present, the sulfide, which is either a sulfide melt or a solid sulfide mineral phase, depending upon temperature and composition, concentrates the chalcophile elements relative to the silicate liquid (Naldrett et al., 1984; Stavast et al., 2005). These sulfides that are concentrated in chalcophile elements host the bulk of the Au, Ag and Cu budget for a range of basaltic to dacitic hydrous magmas (Stimac and Hickmott, 1995). Possibly, the sulfides hold clues to the pre-mineralized metal content and metal ratios of the original source magma of large ore bodies, such as those of Yerington, Nevada and Yanacocha, Peru.

Figure 1 – Location map of the two areas of study

The Yerington, Nevada, ore district is located about 60 km due east of Lake Tahoe and contains porphyry Cu (Mo), Cu skarn, Fe-oxide and Cu-sulfide ores, as well as Cu-Au-Fe oxide lodes. All of these types of deposits are directly associated with the Yerington Batholith, which serves as either the host rock or the source of heat and materials to produce mineralization in the aureole of the batholith (Dilles et al. 2000). The batholith was emplaced and crystallized in about 1 m.y. based on the U/Pb zircon ages of 169.4 Ma for the earliest intrusion and 168.5 Ma for the late mineralized granite porphyry dikes (Dilles and Wright, 1986). There are three major episodes of emplacement of the Yerington Batholith: the McLeod Hill quartz monzodiorite, the Bear quartz monzonite, and the Luhr Hill granite with various cogenetic granitic porphyry dikes (Dilles, 1987). The McLeod Hill quartz monzodiorite represents the earliest and most voluminous phase of the batholith, and

the Luhr Hill granite represents the latest phase emplaced in the center of the batholith (Dilles, 1987). The granite porphyry dikes are cogenetic with the Luhr Hill granite and are temporally and genetically associated with the porphyry copper and copper skarn mineralization (Dilles and Proffett, 1995; Dilles, 1987; Dilles et al., 2000). This production and geologic resources of the district are ~6 Mt of Cu in porphyry and skarn settings from sulfide ores grading ~0.5 wt% Cu and greater than 100 Mt of Fe and 0.5 Mt of Cu in oxide ores (Dilles and Proffett, 1995; Dilles et al., 2000). The magmatic-hydrothermal porphyry copper and skarn ores derived from the Yerington batholith are extremely low in gold content (<2 ppb Au) although iron oxide-copper-gold replacement and lode deposits produced by non-magmatic ore fluids contain significant gold (Dilles and Proffett, 1995; Dilles et al., 2000). Estimates by Dilles (1987) of temperature and fO_2 conditions in the Yerington batholith are shown in Figure 3. All samples examined in this study from the Yerington system are taken from two units of the Yerington batholith: the McLeod Hill quartz monzodiorite, and the Bear border granite.

The Yanacocha Volcanic Sequence (YVS), located in the Andes of northern Peru, approximately 20 km north of the town of Cajamarca, is home to one of the world's largest and most productive gold districts. Yanacocha is a high-sulfidation epithermal mineral system with more than 50 million ounces of gold in oxide ores and an unknown resource of gold and copper in sulfide ores (Longo and Saderholm, 2002). Formation of the YVC began about 14.6 Ma with the eruption of pyroxene-hornblende andesite lavas and continued through a series of lavas, ignimbrites and porphyry dikes until about 8.4 Ma (Longo, 2005). The bulk of the gold ores were deposited between

11 and 8.4 Ma based on Ar-Ar ages on associated hydrothermal alunite (Longo, 2005). The dominant rock type in the YVC is a porphyritic feldspar andesite to dacite, which occurs as lava flows or domes, but is not the preferred host for mineralization (Turner, 1999). The dominant rocks hosting mineralization are andesitic to dacitic strata of pyroclastic or phreatic origin that have undergone massive "vuggy" silica alteration and oxidation. The youngest units of the Yanacocha Volcanic Sequence (YVS) are 8.4 Ma old dacite dikes and associated ignimbrites that are not altered and shortly post-date the youngest hydrothermal activity (Longo, 2005). The temperature and fO_2 conditions for Yanacocha magmas are estimated in Table 1 and Figure 3 on the basis of Fe-Ti oxide compositions following the methodology of Buddington and Lindsley (1964). Within the Yanacocha district, four main units of the YVS were sampled: the lower pyroxene hornblende andesite (Lpha), the Maqui Maqui ignimbrite (MMI), the upper pyroxene hornblende andesite (Upha), and the San Jose ignimbrite (SJI). The lower pyroxene hornblende andesite (14.6-13.1 Ma) is a flow-foliated pyroxene hornblende andesite containing indicative abundant green augite. The Maqui Maqui ignimbrite (12.5 Ma) is a highly mineralized section of the YVS and can be identified by a noticeable lack of pyroxene, as well as abundant broken phenocrysts. Directly above the Maqui Maqui Ignimbrite is the upper pyroxene hornblende andesite (12.3-11.5 Ma), a pyroxene hornblende andesite very similar to the lower pyroxene hornblende andesite, but with greater abundance of hornblende. On top of the upper pyroxene hornblende andesite is the San Jose ignimbrite (11.5-11.2 Ma), a major eruptive and highly mineralized sequence of the YVS that can be found extensively

throughout the district. All age data are from Longo (2005). Temperature and fugacity estimates for the YVS are found in Table 1.

The unit underlying the YVS, a layer of biotite tuff, was also sampled in this study. The biotite tuff (15.51-15.15 Ma) is a biotite dacite pyroclastic sequence that pre-dates both the mineralization and the Yanacocha Volcanic Sequence.

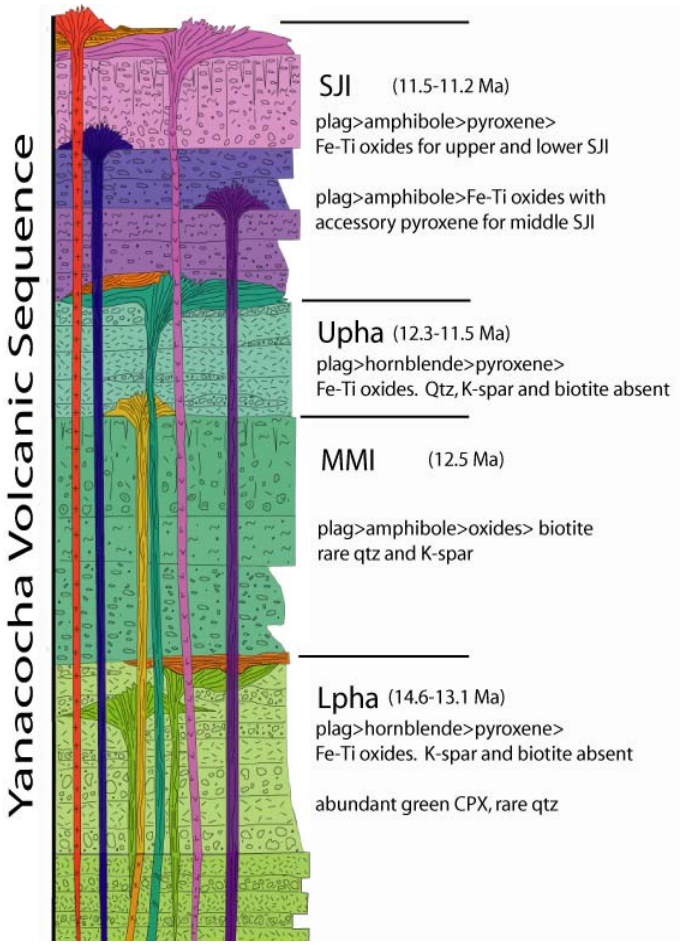

Figure 2 - Columnar section of the Yanacocha Volcanic Sequence, from Figure 2.2 of Longo (2005).

Table 1 – Representative Fe-Ti Oxide Compositions for the Yanacocha Volcanics, Peru

Unit	SJI	Upha	SJI	Lpha	Upha	MMI
Sample	CB-30	DN-30	SJS-79A	CR-3	DN-7	DN-53
Estimated T (°C)	629	731	605	743	614	665
ΔNNO log fO_2	1.8	1.18	1.76	0.4	1.9	1.07
Absolute log fO_2	-16.4	-14.3	-17.3	-14.8	-16.8	-16.2

Analysis by Matthew Harper (written communication, 2005) at Oregon State University using a Cameca SX-100 electron microprobe with natural and synthetic standards. Mark Ghiorso's MELTS solution model (written communication, 2005) was used to estimate temperature (T ^{0}C) and oxygen fugacity (fO_2, both logarithm of absolute fugacity and logarithm of position relative to the Ni-NiO or NNO buffer) of equilibrium of the oxide minerals in the magma (see text). Temperatures are underestimated by MELTS by up to 150°, but oxygen fugacities are relatively robust. Complete electron microprobe data for Fe-Ti oxides can be found in Appendix Table 5.

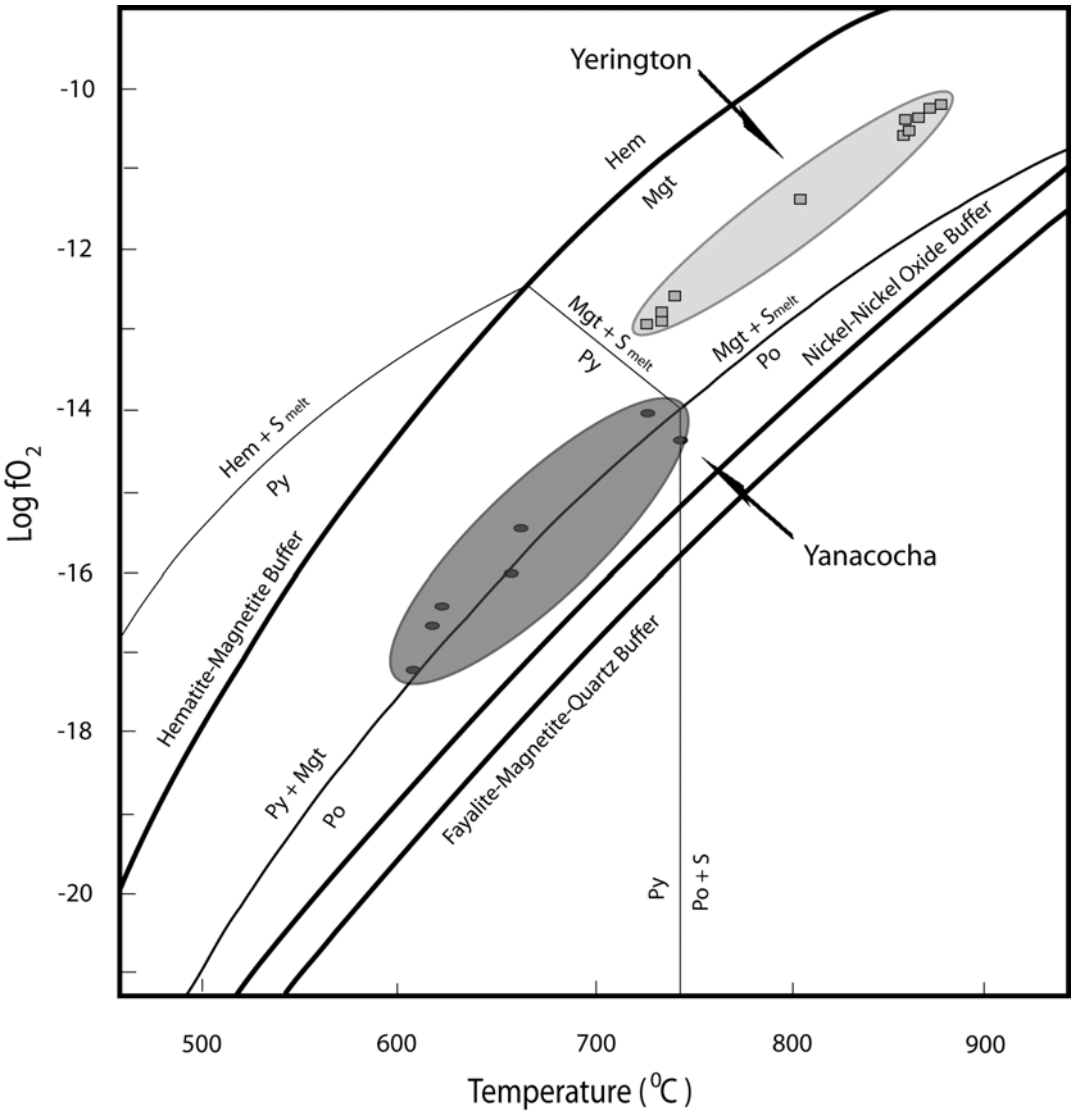

Figure 3 – Temperature-oxygen fugacity (T-fO_2) diagram modified from Whitney and Stormer (1984) and Dilles (1987) showing the approximate fields that the Yerington and Yanacocha rocks occupy with respect to the Fe-S system. The diagram is calculated at a pressure of 2 kilobars. Yerington data are from Dilles (1987). Yanacocha, data are from Table 1 and M. Harper, unpublished data.
Abbreviations: Hem – Hematite Mgt – Magnetite S – Sulfur Py – Pyrite Po – Pyrrhotite

Sulfide stability

The stable sulfide species found within a rock unit can be a good indicator of temperatures, fugacity and cooling history. Magmatic sulfides equilibrate to the stable sulfide species based on available metals and, more importantly, the temperature and the oxygen and sulfur fugacity of the host systems. As shown in Figure 3 the Yerington system is an oxidized system with an oxygen fugacity of magma approximately 2 log units > NNO, whereas the Yanacocha system, in comparison, is slightly less oxidized with a oxygen fugacity 0-2 log units > NNO. The sulfides identified in this study are listed below in Table 2 next to their upper limit of temperature stability.

Table 2 – Magmatic Sulfides and Their Temperature Limits

Mineral	T (^{o}C)	Igneous Rocks
Pyrite	742	Yanacocha
Pyrrhotite	1190	Yanacocha
Chalcopyrite	547±5	Yerington and Yanacocha
Bornite	1100	Yerington
ISS*	880	Yanacocha

Upper temperature limits of sulfide stability for the sulfides identified in the study, data taken from Barnes (1979). The right column shows in which ore complex each type magmatic sulfide was found.
*Intermediate Solid Solution, $(Cu,Fe)_{1+x}S$

Since the Yerington batholith was a slowly cooling igneous body, it contains chalcopyrite and bornite composition magmatic sulfides. Dilles (1984) proposed that these chalcopyrite plus bornite sulfide assemblages were derived through cooling and recrystallization below ~547 ^{o}C from a higher temperature Cu-Fe sulfide mineral called intermediate solid solution (ISS). All the sulfide samples analyzed in this study from the Yerington batholith were of chalcopyrite composition. The Yanacocha

Volcanic System contains ISS, chalcopyrite, pyrrhotite, cubanite, and pyrite; pyrrhotite, ISS, and possibly pyrite can form at magmatic temperatures, but chalcopyrite and cubanite are sub-solidus phases derived from ISS and pyrrhotite. Evidence for the magmatic nature of these sulfides can be seen in photos of the samples in Figure 4. No secondary structures (cracks) were observed leading to or impinging upon the sulfides selected. The sulfides are completely encased within a host silicate mineral, suggesting that as the magma cooled, the silicate mineral grew around and encapsulated the sulfide, where it remained undisturbed from outside processes. The occurrence of a four sulfide magmatic suite (ISS, chalcopyrite, pyrrhotite, and pyrite) similar to what is seen in the Yanacocha district, was seen by Hook (1995) in the volcanic rocks south of the Bingham, Utah, copper district and is a function of the volcanic nature of emplacement and varied cooling histories of each rock unit. Pyrite is generally a hydrothermal sulfide, but Figure 3 illustrates how this assemblage of magmatic sulfides is possible; the Yanacocha sulfide stability range spans the pyrite-pyrrhotite boundary at 742°C using the calculated T-fO_2 conditions.

Methods

Location of Sulfide Grains

The sulfide inclusions were located in polished thin sections of the samples from the Yerington and Yanacocha complexes using a reflected light microscope. Thin sections from five of the main units of the Yanacocha Volcanic Sequence and two units of the Yerington batholith were studied for the occurrence of magmatic sulfides (Table 3). Magmatic sulfides were selected as encased sulfides within a

visibly homogenous host silicate crystal, away from secondary structures or cleavage faces. The vast majority of sulfides for the Yanacocha complex were located in plagioclase feldspars, with a few trapped in clinopyroxene and orthopyroxene. All of the Yerington sulfides were located in potassium feldspars. Below are photographs taken of some of the magmatic sulfides used in this study (Figure 4). Once the magmatic sulfides were located and photos of each were taken, the sulfides were then placed in the electron microprobe at OSU to obtain the major element (Cu, Fe, and S) compositional data.

The sulfides located in the Yerington samples ranged in size from ~7 μm to ~13 μm diameter. The sulfides in the Yanacocha samples were generally smaller than the Yerington sulfides but ranged from ~2 μm to ~20 μm diameter. The major element data collected from the electron microprobe on the samples was used to determine the type of sulfide and is summarized in Table 3, along with the total amount of samples from the different units studied. Compositional names were established by the stoichiometry of the major elements.

Table 3 – Sulfide Mineral Occurrence by Rock Unit

Unit	Total Sulfides	Types of Sulfide
Yerington Batholith	9	Cp
Yanacocha total	34	ISS, Cp±Cb±Po, Py
San Jose Ignimbrite	1	Cp
Upha	2	Py
Maqui Maqui Ignimbrite	5	Po, Cp, ISS
Lpha	23	Po, Cp, ISS
Biotite Tuff	3	ISS, Cp±Cb±Po, Py

Number and type of located sulfides within the Yerington batholith and each individual rock unit of the Yanacocha Volcanic Sequence. Abbreviations: Po – Pyrrhotite, Py – Pyrite, Cp – Chalcopyrite, ISS – Intermediate Solid Solution, Cb – cubanite (± refers to a determined composition between minerals)

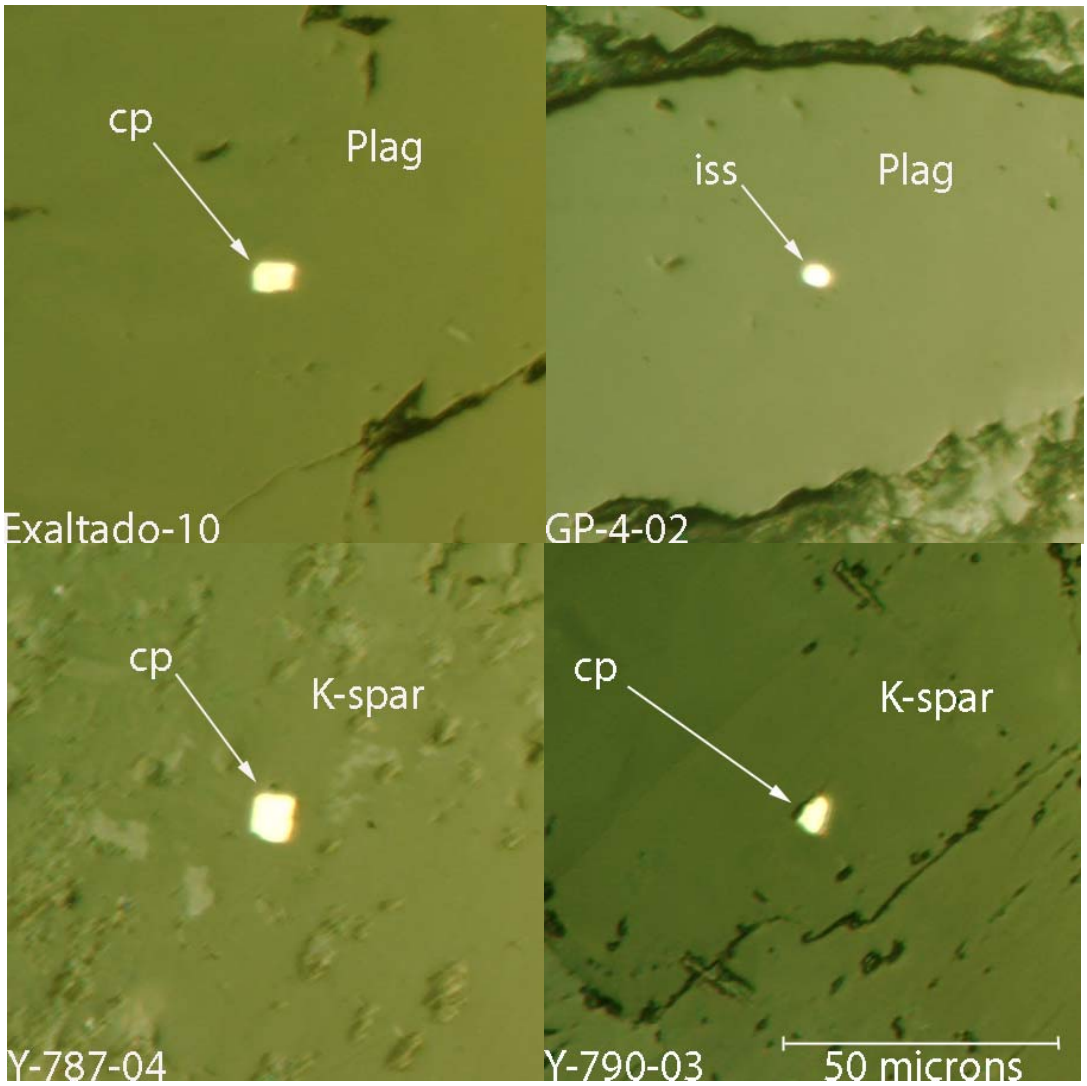

Figure 4 - Examples of Yanacocha sulfides hosted in plagioclase feldspar (Plag, top) and Yerington sulfides hosted in potassium feldspar (K-spar, bottom). The scale bar located in the bottom right corner applies to all photos. Abbreviations: cp – chalcopyrite; K-spar – potassium feldspar, Plag -plagioclase

LA-ICPMS Analysis

The work preformed by Halter et al. (2002b) on major and trace element analysis of melt inclusions via LA-ICPMS describes a method of how a melt inclusion of lesser diameter than the laser beam could be analyzed. Their method is utilized for the LA-ICPMS work on sulfide inclusions during this study and is described as used below.

Trace metal and major element analysis for this project was conducted using LA-ICPMS at Oregon State University, a Lambda Physik DUV 193 Excimer laser connected to a VG Excel Quadrupole ICP-MS and pumping helium-argon gas as a carrier. Standard and unknown samples were analyzed with a 30-micrometer laser spot diameter using a pulse rate of 2 Hertz. Data collection for all samples included 45 seconds for background collection with laser off, 45 seconds of peak collection with the laser firing, and 45 seconds of washout time (Figure 11). The initial 45 second background is subtracted from the peak count rate to obtain the sample count rate. The LA-ICPMS at OSU was used two separate times during this project. In the first use, the dwell time of the laser was set at 10 microseconds (ms) per element and the elements and isotopes tested were as follows: ^{29}Si, ^{33}S, ^{43}Ca, ^{57}Fe, ^{58}Fe, ^{59}Co, ^{60}Ni, ^{65}Cu, ^{66}Zn, ^{75}As, ^{78}Se, ^{95}Mo, ^{109}Ag, ^{121}Sb, ^{197}Au, ^{202}Hg, and ^{208}Pb. During the second ablation, only ^{65}Cu, ^{66}Zn, ^{109}Ag, ^{197}Au, and ^{208}Pb were counted. The dwell time was held at 10 ms for all elements except ^{197}Au, which was changed to 100 ms in order to increase total counts.

All metal concentrations reported (excluding Cu) are derived from these data. For the calibration of the LA-ICPMS at OSU, the MASS sulfide standard, manufactured by the USGS was employed. The MASS standard consists of CuFeZn sulfide melted with ~100 ppm each of several trace metals; the melt was quenched, ground finely, and pressed into a pellet that is apparently homogeneous, with the possible exception of gold, for which there is a small "nugget" affect observed at laser beam diameters less that 50 micrometers (Wilson et al., 2002).

Because this was a newly created standard and the first use at the Oregon State University LA-ICPMS lab, the reproducibility and accuracy of analysis of this standard and comparison with the results of Wilson et al. (2002) was critical for accurate analysis of the sulfides in this study. Replicate analysis on MASS was performed at OSU to ensure the standard was well suited and reproducible at the OSU lab. When compared to the results of Wilson et al. (2002) for the same elements and similar spot sizes (Figure 5), the percent relative standard deviation at OSU was, in all cases, lower than the USGS published results. Figure 6 shows the agreement of critical element ratios detected in the USGS published results and OSU data (average of all measurements). These data showed that the standard data was reproducible at the Oregon State University LA-ICPMS lab, but required a laser diameter of 30 microns (μm) or greater to maintain accurate detection capabilities.

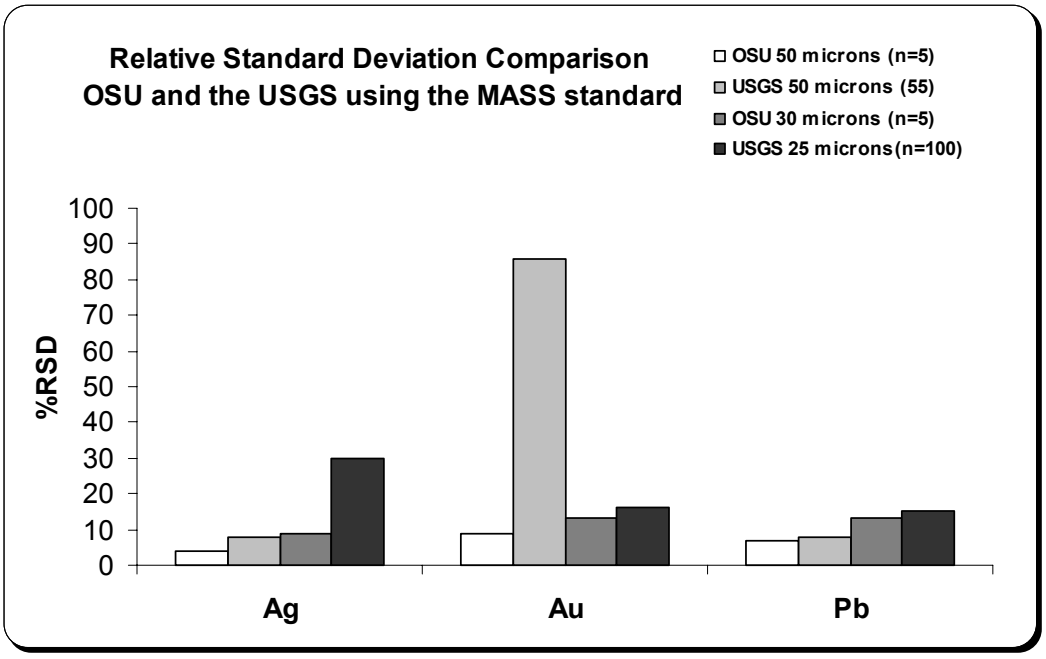

Figure 5 – Graph showing the reproducibility of the MASS standard at Oregon State University, indicating the OSU lab is suitable for this type of sulfide study. The large relative standard deviation (RSD) for gold shows the difficulty in homogenization due to the "micro-nuggeting" tendency of the element.

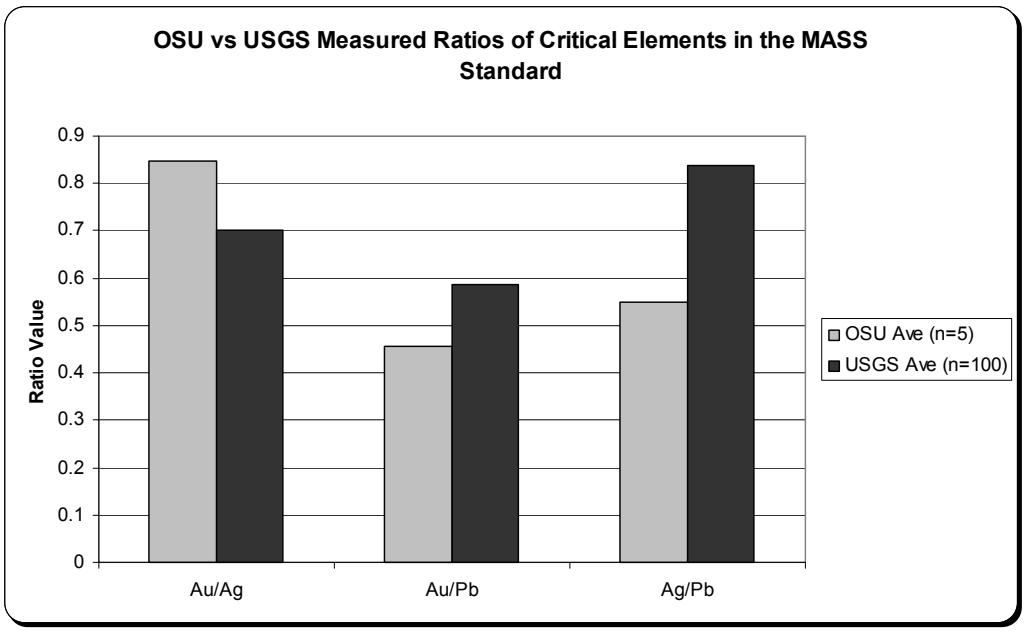

Figure 6 – Graph comparing the agreement of the MASS standard ratios detected at Oregon State University and those published by the USGS.

Since the majority of the magmatic sulfides used in analysis were less than 30 μm diameter, a reliable technique for evaluation of sulfides less than 30 μm was crucial. The technique outlined by Halter et al. (2002b) for trace element analysis using laser ablation of melt inclusions was modified and employed for the analysis of sulfide inclusions in this study and is described below.

To acquire data on the micron-sized sulfides, the following steps were applied: 1) the Cu, Fe, S and SiO_2 content of each sulfide was analyzed by electron microprobe; 2) the host mineral of the magmatic sulfide was analyzed via LA-ICPMS to obtain a host background signal; 3) the area within the host mineral containing the sulfide is then ablated; 4) the background signal of the host mineral is subtracted from the signal obtained from the sulfide and host mixture, leaving only the signal from the sulfide inclusion. The method is diagrammed in Figures 7 and 8 below. The method used makes the following assumptions:

A) The host mineral is relatively homogenous
B) The host mineral has approximately the same elemental composition directly surrounding the sulfide, compared to where it was analyzed nearby for background

The first two assumptions mentioned above are made because the sulfide inclusions sampled were only chosen from hosts that appeared to be homogenous under reflected light and, compositionally, were analyzed by the electron microprobe. Areas ablated on the hosts were chosen away from cleavages and impurities.

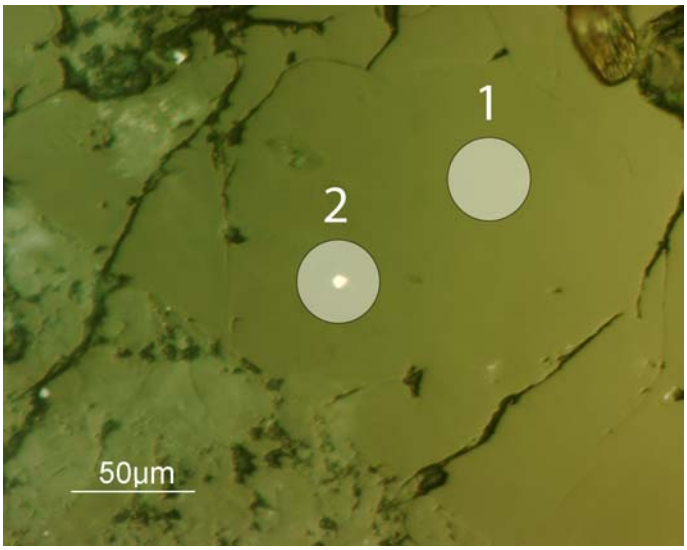

Figure 7 - Microscope view of the Halter et al. (2002b) ablation diagram as applied to magmatic sulfides. This chalcopyrite crystal is hosted within plagioclase feldspar from the Yanacocha volcanics in sample CR-3-01. The laser ablation spot size as represented by the circle is 30 microns in diameter, the size used in this study. The first hole (1) is ablated in the host silicate mineral; the second hole (2) is centered above the sulfide inclusion to obtain a signal from the mixture of matrix and sulfide. The host silicate is subtracted out from the mixture signal to leave only the signal from the sulfide inclusion for the final data.

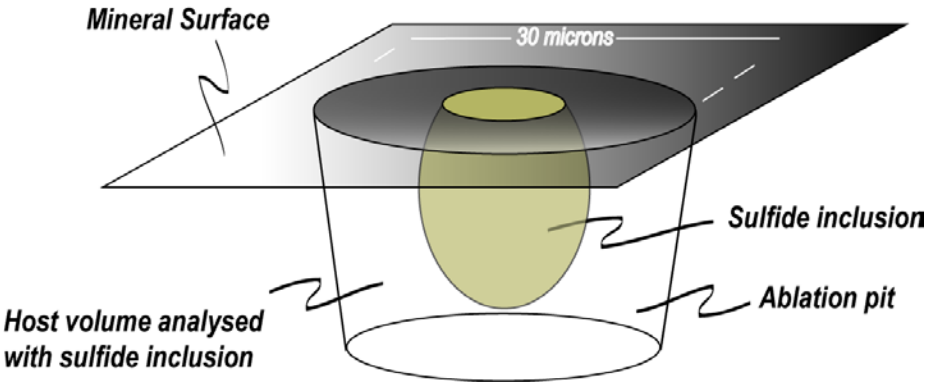

Figure 8 – A Three dimensional diagram modified from Halter et al. (2002b) schematically showing the procedure for ablating a sulfide inclusion that is smaller than the laser diameter. In this study, the technique was applied to sulfide inclusion analysis. This diagram corresponds to the second ablation (2) in Figure 7.

Detection Limits

Using the MASS standard for the Oregon State University LA-ICPMS, the detection limits were calculated and are shown for a 30-µm beam below in Figure 9. Detection limits are based on three times the standard deviation of the background counts per second, times the concentration of the element, divided by the counts per second (3σ). The unknown sulfide samples were derived from the relationship of peak to background in the sulfides and peak to background relationships in the known sulfide standard, as outlined in Halter et al. (2002b), and shown in the equation below. It is important to note that the smaller the sulfide, which generally has a lower number of total counts for each element, the higher the detection limit is for that individual sulfide. Figure 9 shows an average of individual detection limits for all the sulfides.

$$\text{Detection Limit (ppm)} = \frac{3\sqrt{B_i}}{\left(B_i / S_p\right)}$$

B_i = Background of the ICPMS (cps)

S_p = Sulfide standard peak (ppm)

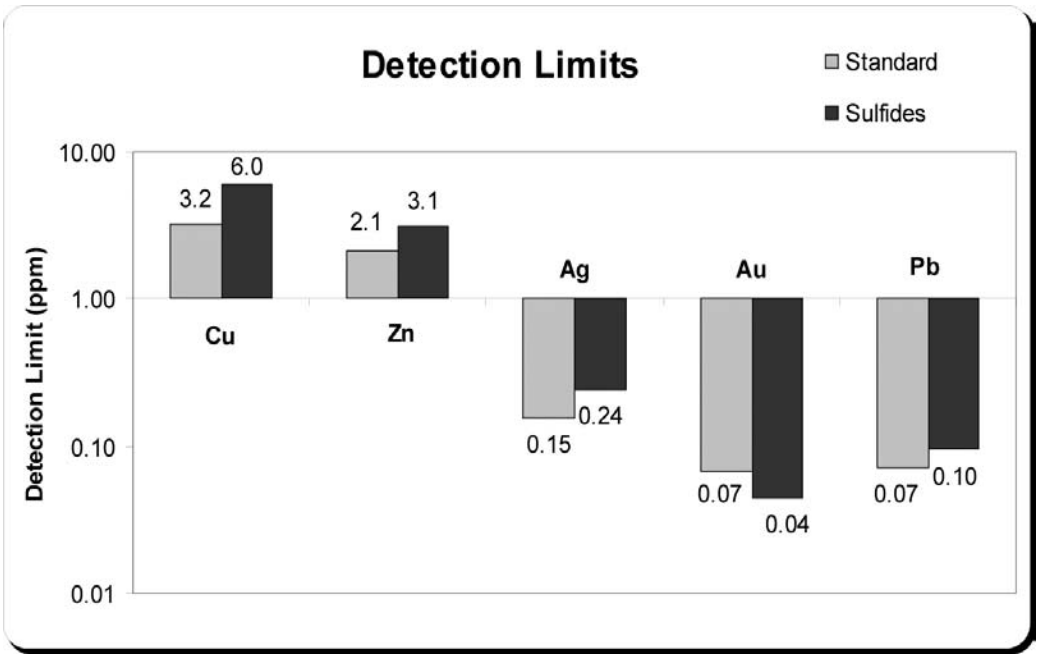

Figure 9 – Average detection limits (3σ of background cps) for elements of interest from the MASS standard and the unknown sulfides. The sulfide average taken is the average detection limit of each element for all sulfides ablated, and each detection limit is calculated for a 30 μm diameter beam.

Determining Concentrations within the Sulfides

The total area of the sulfide, of which only one slice on the surface can be seen in thin section, must be estimated in order to assign metal concentrations to the sulfide itself, and not the entire ablated area. The first step in doing this is to directly subtract the counts per second for each element measured in the host mineral from the counts per second of each element measured from the ablation of the sulfide. This removes all elemental counts that could be contributed directly by the host mineral surrounding the sulfide and part of the first ablation (1), as shown in Figure 7. For the second step, i.e., the determination of the metal concentrations within each sulfide, two different methods were evaluated, the "half-cylinder method" and the "Cu-normalization method".

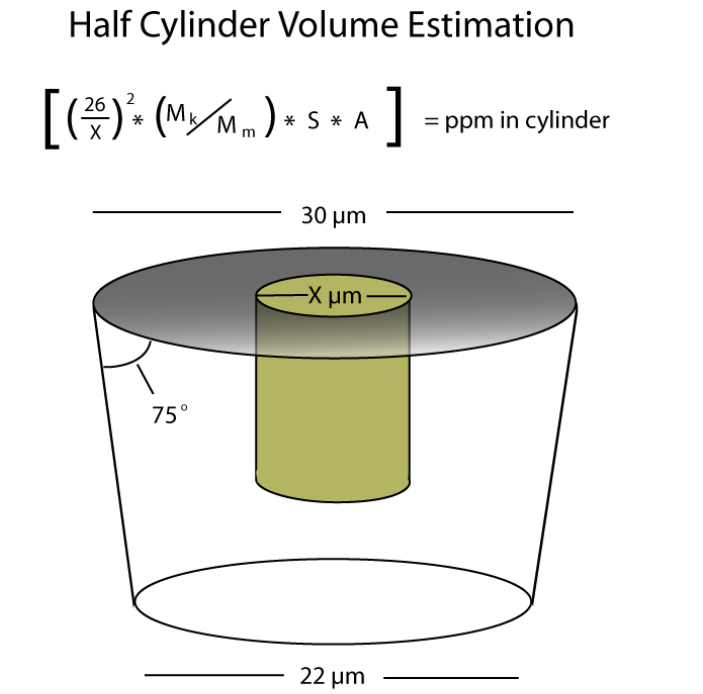

Figure 10 – Diagram showing the "half-cylinder" estimation procedure to determine the concentrations of metals within the sulfide alone and not the surrounding host mineral.

The first method analyzed, the "half-cylinder method," was based upon the radius of the sulfide seen on the surface, estimating the sulfide to be a half-cylinder of that seen at the surface, as shown above in Figure 10. This method produced very inconsistent metal concentration data, and after close examination of the ablation profiles of each sulfide, the reason for failure was discovered. Figure 11 below shows two examples of ablation profiles of sulfides used in this study, CA-1-01 and DN-30-02. The differences in these ablation profiles show how one sulfide (CA-1-01) has a

very shallow depth and is quickly ablated, returning the signal quickly back to the background levels. DN-30-02 shows a fairly consistent signal throughout the ablation until the laser is turned off. This particular sample had a deep profile reflecting a substantial sulfide thickness and much higher overall volume than CA-1-01. These inconsistencies in the sub-surface of the sulfide made the "half-cylinder" estimations invalid for this study.

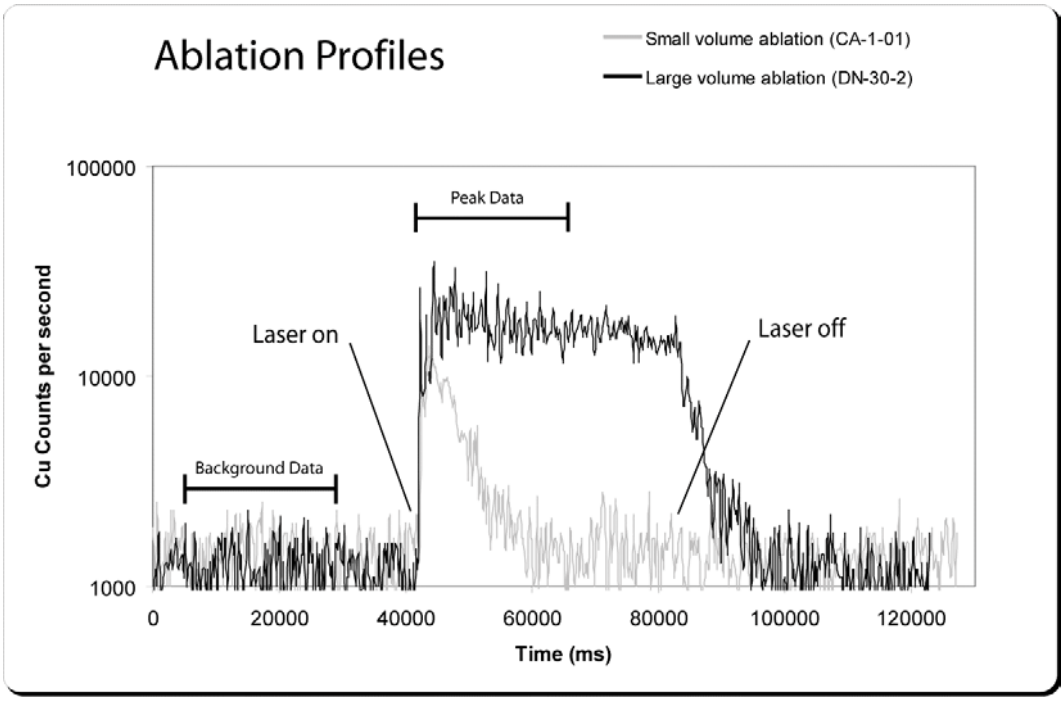

Figure 11 – Ablation profiles of small and large volume sulfides. The large volume ablation profile of sample DN-30-2, showing the data collection periods for background and peak compared to the small volume ablation profile of sample CA-1-01. When this type of small volume ablation profile is seen, the sulfide had very little depth and was fully ablated within a few seconds; therefore making a half cylinder estimation invalid to determine the volume of the sulfide.

In the second method, the "Cu-normalization method," Cu concentrations from the electron microprobe are used as an internal standard for the ICPMS. This procedure is based upon the number of counts of Cu from the ICPMS and the wt% Cu detected by the electron microprobe normalized to 100% Cu-Fe sulfide (silicate-free, Appendix Table 2). The wt% Cu from the electron microprobe and the obtained counts of Cu from the LA-ICPMS were used, along with the known ratio of counts to concentration of the MASS standard, to scale counts Cu into a known concentration for Cu for the sulfide sample. With a known concentration of Cu in the sulfide, the remaining metals (Au, Ag and Pb) were scaled into concentrations by the measured counts relationship to Cu. The formula shown below demonstrates how Au concentrations were calculated in this study. The same method was applied for Ag and Pb (Longerich et al., 1996).

$$\text{ppm Au} = \left(\frac{\frac{\text{ppm Cu}}{[\text{Microprobe}]}}{\frac{\text{cps Cu}}{[\text{LA-ICPMS}]}}\right)_U \left(\frac{\frac{\text{cps Au}}{[\text{LA-ICPMS}]}}{1}\right)_U \left(\frac{\frac{\text{ppm Au}}{[\text{Standard}]}}{\frac{\text{ppm Cu}}{[\text{Standard}]}}\right)_{STD} \left(\frac{\frac{\text{cps Cu}}{[\text{LA-ICPMS}]}}{\frac{\text{cps Au}}{[\text{LA-ICPMS}]}}\right)_{STD}$$

U = Unknown Sample

STD = MASS Standard

[ ] = Data Source

External estimates of Cu weight percent for each individual sample are needed in this method to assign concentrations to Au, Ag and Pb. For most samples, Cu was determined by electron microprobe (see Table 5 above and Appendix Table 2), but for the few samples that were not analyzed, a weight percent copper was assigned based on the type of sulfide mineral and the amount of copper found in like minerals of the same unit. Absolute concentration errors estimates were calculated as shown in Bevington (1969) and are based upon the total number of counts obtained from the

LA-ICPMS on each individual element of each sulfide. For all elements except Au, errors are listed as averages from the individual calculations (Table 6), whereas Au is listed individually by sulfide.

Results

Electron Microprobe analysis

The electron microprobe at Oregon State University, a Cameca SX-100, was used for the major element analysis and composition of the magmatic sulfides in this study. The microprobe column conditions at the times of analysis were 15keV, 50nA, with the beam size set at 2 μm. The signals used for each element detected were as follows: Si-Kα, S-Kα, Fe-Kα, and Cu-Kα. A chalcopyrite standard was used for the Cu data, and a pyrite standard for Fe and S. Because the micrometer-sized sulfides analyzed were hosted within a silica-rich silicate mineral, a partial silica signal was expected along with the chalcophile elements. The minimum silica signal obtained at each sample was used as an indicator of the optimal beam position above the silica-void sulfide. Where silica was detected by the electron microprobe, the beam was also analyzing the silicate host mineral, and the totals are expected to be low. Typical electron microprobe procedures were followed for analysis, and representative samples are shown in Table 4; Appendix Table 4 gives complete data, and atomic proportions of Cu, Fe, and S.

Table 4 - Representative Electron Microprobe Samples

		Weight Percent					Determined
Sample	Unit	SiO2	S	Fe	Cu	Total	Mineral
OCU-3-01	Upha	2.1	53.7	47.3	0.3	103.4	Py
DN-30-02	MMI	9.5	33.4	52.1	2.9	98.0	Po
Exaltado - 02	Lpha	18.8	24.4	32.8	12.0	88.0	Cp+Cb?
GP-4-03	Lpha	6.7	26.0	21.6	26.9	81.3	Cp
Y-787-01	YB	32.5	24.0	18.5	20.4	95.4	Cp
Y-793-01	YB	7.5	33.0	28.4	35.4	104.3	Cp

Representative Yerington and Yanacocha samples of the major element analysis from the OSU electron microprobe at OSU, a Cameca SX-100. For complete data, see Appendix Table 2. Abbreviations: see Table 3.

Data from the electron microprobe was used to determine the amount of copper and the type of sulfide mineral for each sample. However, some of the sulfides analyzed appear to have a sulfur deficiency and do not stoichiometrically fit near the reference sulfides of chalcopyrite, pyrite, ISS, cubanite, or bornite (Figure 12). Keith et al. (1997) suggested that these sulfur deficiencies occur in sulfides when the sulfur is replaced by oxygen, forming a Fe-oxide residue on the outside of the sulfide. Because only the amount of Cu was used in the scaling process for this study, the normalization is not effected by the sulfur deficiencies of a few of the samples. Determined compositions of some samples fell stoichiometrically between the reference sulfides and are noted by combinations of the closet reference sulfides (Figure 12 and Table 4). It is possible that the measured cubanite (a non-magmatic sulfide mineral) and non-stoichiometric sulfide data is obtained from a combination of signals from sulfides derived through cooling and recrystallization from a higher

temperature Cu-Fe sulfide mineral, as mentioned earlier in the case of the Yerington chalcopyrite-bornite assemblages.

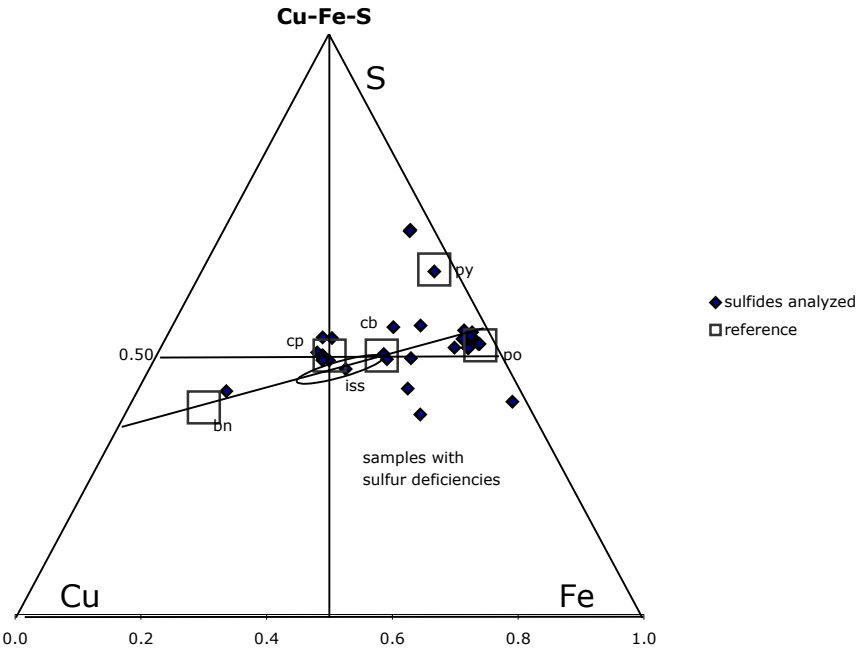

Figure 12 – Diagram depicting the Cu, Fe and S composition (silicate-free) in atomic proportions of the magmatic sulfides analyzed (Appendix Table 2). The locations of common mineral species are shown for reference. Abbreviations are given in Table 3.

LA-ICPMS analysis

As described in the *Methods* section, Au, Ag and Pb were scaled into concentrations by the measured counts relationship to Cu (Table 5). Those sulfides

with lower Cu concentration such as pyrite and pyrrhotite, as well as smaller volume sulfides, inherently have a higher amount of error associated with them. Where the ablated material was dominated by the silicate host, the metal signals are smaller and the detection limit increases.

The calculated trace element compositions of the magmatic sulfides show very large ranges of concentrations for Au and Ag for both studied ore districts. The Au content in magmatic sulfides ranged from less than detection limit (n=4) to detectable amounts of 5.4 to 131 ppm (n=5) at Yerington, and from less than detection limit (n=17) to detectable amounts of 0.44 to 494 ppm (n=17) at Yanacocha. Silver concentrations for Yerington and Yanacocha ranged from 29 to 2373 ppm (n=7, n= 2 below detection limit) and 0.36 to 6932 ppm (n=20, n=14 below detection limit), respectively.

Table 5 - Metal Concentrations of Magmatic Sulfide

					Microprobe				LA-ICPMS			
	Size	**Rock**	**Host**		wt%	wt%	wt%	wt%*	ppm	ppm		ppm
	(μm)	**Unit**	**mineral**	**Sulfide**	**S**	**Fe**	**Cu**	**Cu**	**Ag**	**Au**		**Pb**
SJS-79A-01	5	SJI	Plag	Cp	38.1	27.5	34.4	34.4	192	0.61	±0.62	<0.1
OCU-3-01	20	Upha	Plag	Py	53.0	46.7	0.3	0.3	29.9	<0.05		3360
YSBD-01	9	Upha	Plag	Py	62.5	37.5	0.0	0.0	<0.24	<0.05		<0.1
DN-7-01	5	MMI	Plag	Cp		No data		36.4^	<0.24	30	±0.51	16860
DN-7-03	3	MMI	Plag	Cp	35.2	28.4	36.4	36.4	206	<0.05		427
DN-7-04	4	MMI	Plag	Cb+Po?	25.9	52.6	21.5	21.5	6930	207	±1.3	0
DN-30-01	6	MMI	CPX	Po	39.0	60.7	0.3	0.3	<0.24	2.26	±0.82	<0.1
DN-30-02	4	MMI	Plag	Po	37.8	58.9	3.3	3.3	15.1	0.44	±0.82	6
Exaltado-2	9	Lpha	Plag	Po+Cb?	35.3	47.4	17.3	17.3	112	<0.05		<0.1
Exaltado-5	5	Lpha	Plag	Cb+Po?	40.9	41.5	17.6	17.6	725	3.86	±0.82	<0.1
Exaltado-6	5	Lpha	Plag	Cp		No data		35.5	<0.24	<0.05		11200
Exaltado-9	3	Lpha	Plag	Po	37.7	59.1	3.2	3.2	<0.24	<0.05		<0.1
Exaltado-10	10	Lpha	Plag	Cp	34.9	29.1	36.0	36.0	38.0	4.65	±0.63	51
Exaltado-11	6	Lpha	Plag	Po		No data		2.5^	<0.24	42.6	±0.54	64
C Atazaico-01	8	Lpha	OPX	Po	28.7	70.9	0.4	0.4	<0.24	<0.05		<0.1
C Atazaico-02	3	Lpha	Plag	ISS		No data		15.0^	541	<0.05		<0.1
C Atazaico-03	4	Lpha	Plag	Po		No data		2.5^	<0.24	<0.05		951
C Atazaico-04	2	Lpha	Plag	Po		No data		2.5^	57	<0.05		100
C Atazaico-05	4	Lpha	Plag	Cb?	34.7	42.3	23.0	23.0	<0.24	<0.05		<0.1
C Atazaico-06	5	Lpha	Plag	Po	41.0	57.1	1.9	1.9	20	<0.05		860
C Atazaico-07	10	Lpha	Plag	Po	38.6	61.0	0.4	0.4	11	<0.05		8
C Atazaico-08	4	Lpha	Plag	Cb?	41.4	47.4	11.2	11.2	<0.24	21.40	±0.75	344
C Atazaico-09	6	Lpha	Plag	Cp	1.0	93.9	5.0	5.0	61	<0.05		<0.1
GP-4-01	4	Lpha	Plag	Cb?	35.8	41.4	22.8	22.8	257	19.00	±0.71	757
GP-4-02	5	Lpha	Plag	Po+Cb?	30.0	48.6	21.4	21.4	895	177	±0.58	924
GP-4-03	9	Lpha	Plag	Cp	34.9	29.0	36.1	36.1	<0.24	494.4	±0.58	<0.1
CA-1-01	16	Lpha	Plag	Po	38.6	61.3	0.05	0.05	<0.24	0.83	±0.71	<0.1
CA-1-02	7	Lpha	Plag	Po	39.9	58.9	1.1	1.1	<0.24	<0.05		<0.1
CR-3-01	6	Lpha	Plag	Cp	34.1	30.7	35.2	35.2	894	3.95	±0.43	58
CR-3-02	4	Lpha	Plag	ISS	32.7	34.8	32.5	32.5	0.4	<0.05		<0.1
CR-3-03	5	Lpha	Plag	Cp		No data		34.7^	451	1.51	±0.82	28
DN-45-01	5	BT	Plag	Po	39.3	57.4	3.3	3.3	8.1	1.59	±1.16	<0.1
DN-47-02	5	BT	Plag	Py	62.1	37.7	0.2	0.2	3.4	<0.05		<0.1
DN-47-03	8	BT	Plag	Po	37.6	56.1	6.4	6.4	<0.24	80.1	±0.54	<0.1
Y-787-01	11	YB	K-spar	Cp	38.2	29.4	32.4	32.4	29	10.1	±0.63	4520
Y-787-02	12	YB	K-spar	Cp	34.8	29.1	36.1	36.1	345	<0.05		<0.1
Y-787-04	12	YB	K-spar	Cp		No data		35.0^	2370	16	±0.65	36600
Y-790-01	10	YB	K-spar	Cp		No data		35.0^	273	<0.05		712
Y-790-02	9	YB	K-spar	Cp		No data		35.0^	<0.24	131	±0.63	1230
Y-790-03	7	YB	K-spar	Cp		No data		35.0^	142	5.4	±0.56	<0.1
Y-793-01	12	YB	K-spar	Cp	34.1	29.3	36.6	36.6	575	<0.05		<0.1
Y-793-02	13	YB	K-spar	Cp		No data		35.0^	<0.24	<0.05		<0.1
Y-793-03	12	YB	K-spar	Cp		No data		35.0^	214	52	±0.54	677
Ave Error								1.5E-6	0.15	individual		0.121

Metal concentrations obtained by the electron microprobe (middle three columns) and the ICPMS (right four columns). The host mineral, type of sulfide, rock unit and sulfide size are listed in the left four columns; see Figures 2 and 3 for abbreviations.

* Determined by electron microprobe analysis

^ Estimated concentration based upon analysis of similar sulfides of the same rock unit.

Elements also measured in this experiment but not listed in Table 5 are as follows with the approximate detection limits of ppm in parenthesis: Co (2.3), Ni (15.9), As (3.1), Se (13.4), Mo (0.7), Sb (0.2) and Hg (1.3). Due low concentrations, these were not detectable. Zinc (mass 66) was not detected due to a mass interference.

Where Au, Ag and Pb were detectable, the Au/Cu, Ag/Au, and Pb/Cu ratios have been calculated (Figure 13). Yanacocha magmatic sulfides have a higher average Au/Cu, Ag/Cu, and Pb/Cu, but a lower average Au/Ag than the Yerington magmatic sulfides, although all are within a factor of 4 or less and close to analytical uncertainty. The ratios reported are averaged over all samples in each respective ore district. Au/Cu (x10,000) represents the largest discrepancy between the two localities with values of 2.2 and 0.7 for Yerington and Yanacocha, respectively. The second largest difference in the two districts' ratio values was Pb/Cu (x100), with a Yanacocha value of 4.2 and Yerington of 1.4. The Ag/Cu (x1000) values were very close to one another, 2.2 and 1.2 for Yanacocha and Yerington, respectively. The average Au/Ag (x10) ratio or Yerington magmatic sulfides is 0.7, which is higher than the average ratio of 0.2 for Yanacocha.

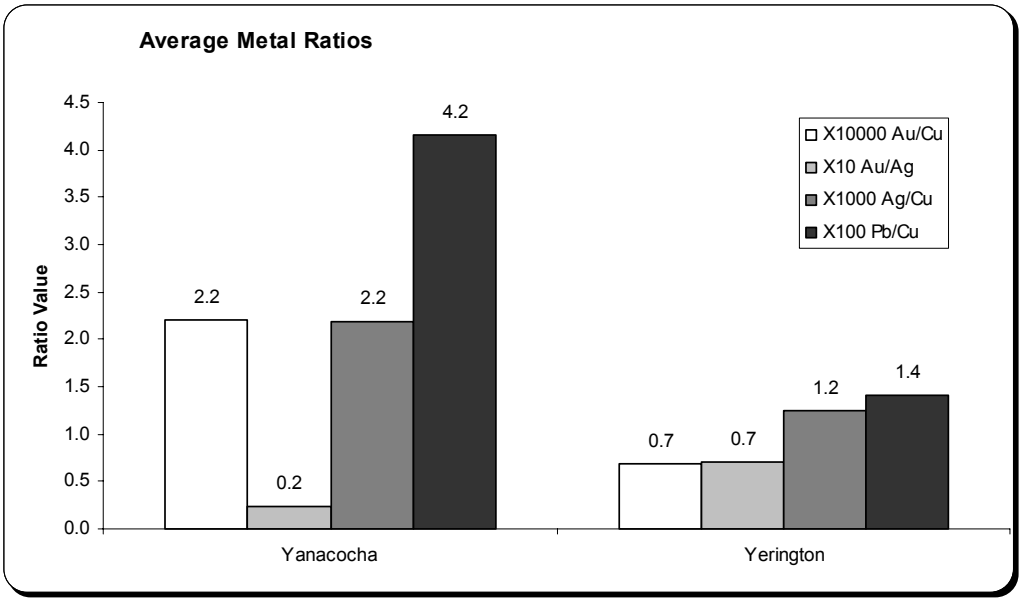

Figure 13 – Graph of the average metal ratios found in the two systems of Yerington, Nevada and Yanacocha, Peru.

The Au/Cu metal ratio for magmatic sulfides obtained in this study can be compared to Au/Cu ratio obtained from magmatic sulfides in the Bajo de la Alumbrera complex, NW Argentina, (Halter et al., 2005) related to porphyry Cu-Au ores (Table 6). Only samples with data above detection limit for Au and Cu were used in this chart.

The absolute Au concentration of the magmatic sulfides obtained by Halter et al. (2005) are lower in general, ranging from 0.21 to 4.33 ppm Au and show much less variance than those obtained by this study. Nonetheless, the Au/Cu ratios (x10,000) obtained in the two studies are very comparable. The Yerington system, which is associated with porphyry Cu-Mo ores that are extremely low in gold content (1 ppb, Dilles and Proffett, 1995), has the lowest average Au/Cu ratio (for samples with

detectable Au) of the three (1.23) and a very consistent range (0.15-3.75). The other two systems, Bajo de la Alumbrera and Yanacocha both have a large range of Au/Cu ratios (0.07 – 36.02 and 0.02 – 17.04, respectively) but similar average ratios (4.64 and 3.96, respectively) for the samples analyzed.

Table 6 – Au/Cu Ratio Comparison

Au/Cu (x10000)			
This study		**Halter et al. 2005**	
Yanacocha		Bajo de la Alumbrera	
SJS-79A-01 (cp)	0.02	BLA67/7/SA3	12.20
DN-7-01 (iss)	0.82	BLA67/7/SA4	20.77
DN-7-04 (iss)	9.61	BLA67/7/SA7	18.10
DN-30-01 (po)	6.87	BLA67/7/SA8	36.02
DN-30-02 (po)	0.13	BLA67/7/SA11	2.55
Exaltado-2 (iss)	0.02	BLA67/7/SA12	0.19
Exaltado-5 (iss)	0.22	BLA67/8/SA2	0.08
Exaltado-10 (cp)	0.13	BLA67/8/SA8	2.41
Exaltado-11 (po)	17.04	BLA67/8/SA9	0.61
C Atazaico-07 (po)	0.28	BLA67/8/SA11	3.24
C Atazaico-08 (iss)	1.91	BLA6778/SA13	0.67
GP-4-01 (iss)	0.83	BLA67/8/SA16	0.16
GP-4-02 (iss)	8.28	BLA67/8/SA18	0.14
GP-4-03 (cp)	13.70	BLA67/9/SA2	2.46
CR-3-01 (cp)	0.11	BLA67/9/SA6	0.07
CR-3-03 (cp)	0.04	ML3/9/SA6	4.33
DN-45-01 (po)	0.48	ML3/9/SA9	0.43
DN-47-02 (py)	2.26	ML3/9/SA11	0.99
DN-47-03 (po)	12.51	ML47/3/SA2	1.61
Average	**3.96**	ML47/4/SA7	0.74
Standard Deviation	5.6	ML47/4/SA14	3.56
		ML47/4/SA16	2.89
Yerington		ML47/5/SA18	1.82
Y-787-01 (cp)	0.31	ML47/5/SA19	8.76
Y-787-04 (cp)	0.45	ML47/5/SA20	0.46
Y-790-02 (cp)	3.75	ML47/6/SA22	0.72
Y-790-03 (cp)	0.15	ML47/6/SA23	2.57
Y-793-03 (cp)	1.48	ML47/6/SA24	2.51
Average	**1.23**	ML47/6/SA26	3.63
Standard Deviation	1.5	**Average**	**4.64**
		Standard Deviation	7.9

Au/Cu ratios (multiplied by 10,000) of magmatic sulfides from Yanacocha and Yerington containing detectable Au compared to Au/Cu ratios from magmatic sulfides from the porphyry-Cu-Au Bajo de la Alumbrera complex in NW Argentina (Halter et al., 2005).

Discussion

Regarding the Method

The goal of accurate determination of Cu, Au and Ag relative ratios in magmatic sulfides for the Yerington and Yanacocha districts appears to have been achieved, given the close agreement with previous work by Halter et al. (2002b) on magmatic sulfide Au/Cu ratios. Because the calculated ratios are not effected by errors associated with scaling elements into concentrations, the results are much more robust than actual concentrations. The methodology followed in this study can be used to provide reliable Au/Cu ratios, even from small sulfides with diameters <10 μm, for sulfides containing more than about 0.5 ppm Au.

The methods used for determination of metal concentrations (specifically Au, Ag, and Pb) within sulfides from the Yerington and Yanacocha ore districts must have a considerable amount of unknown error associated with it, as the metal concentrations (Au in most cases) calculated in some sulfides appear to be somewhat unrealistically high. Within these anomalously high samples, no good correlations can be drawn from the scaling numbers (related directly to size), rock unit, or the concentrations of any other elements determined. It is interesting that most of the large Au anomalies appear in intermediate composition sulfides, but again, no correlation between Cu content or rock unit is visible.

Ore Deposit Metal Ratios

Whereas there may be strong evidence for Au/Cu ratios found in magmatic sulfides matching the bulk ore Au/Cu ratios of large porphyry system at Bajo de la

Alumbrera, as well as preliminary evidence in Elatsite, Bulgaria to follow the same interpretations (Halter et al., 2002a), the evidence in this study cannot draw the same conclusions. The bulk Au/Cu ratio of porphyry Cu-Mo ores from Yerington, Nevada is about 2 x 10^{-7} or about one thousand times lower than those found in the magmatic sulfides. The high sulfidation deposits of Yanacocha, which have proven resources of Au (>50 M oz.) with small amounts of Ag, would need to contain over 3 Mt of Cu to match the Au/Cu ratio found in the magmatic sulfides. At Yanacocha, there is an unknown but large amount of Au, Ag, and Cu within the sulfide ore resources underlying the main economic oxide Au deposits of Cerro Yanacocha (Longo and Saderholm 2002). The oxide ores have been leached of most of their Cu, so the sulfide ores are the best guide. We estimate these to contain about 250 ppm Cu and 0.5 ppm Au for a Au/Cu ratio of 1/500, or Au/Cu x10,000 equal to 20. So, a decisive answer is unknown for the Yanacocha deposit, however, preliminary data suggests a much higher Au/Cu ratio found in the bulk ore than in the magmatic sulfides (Table 7).

Table 7 – Bulk Ore and Sulfide Ratios

Ore Deposit Ratios	**Au/Cu (x10,000**
Yerington Bulk Ore	0.0025
Yerington Magmatic Sulfides	1.6
Yanacocha Bulk Ore	~20
Yanacocha Magmatic Sulfides	5.5
Bajo de la Alumbrera Bulk Ore	4.6
Bajo de la Alumbrera Magmatic Sulfides	4.6

Average Au/Cu ratios (x10000) for the bulk ore as well as the magmatic sulfides for the two ore systems in this study compared with the Bajo de la Alumbrera data from Halter et al. (2002a)

Ore Deposit model

Even though the Cu±Mo porphyry system of Yerington, Nevada, and the high-sulfidation epithermal Au-Cu system of Yanacocha, Peru are very different as types of ore deposits, they share a similar origin. Magmatic fluids, both vapor and saline liquid, are a primary source of metals in a hydrothermal ore deposit (cf., Hendenquist and Lowenstern, 1994). These types of fluids, as well as the associated magmatic and subvolcanic intrusions are ultimately responsible for the creation of the large ore deposits of Yerington and Yanacocha. Figure 14 demonstrates the path of the metal-rich vapor and the spatial relationship of the two styles of ore deposition in the sub-surface. High sulfidation systems, like that of Yanacocha, commonly share many mineralogical, stable-isotope and spatial characteristics with the advanced argillic zones that generally cap porphyry deposits (Sillitoe, 1989; Hendenquist and Lowenstern, 1994). It is unclear whether a Cu-rich porphyry system underlies the Yanacocha high-sulfidation zone, or if a Au-rich high-sulfidation zone has been eroded from the top of the Yerington porphyry, but both scenarios are a possibility to explain the low concentrations of Cu found in Yanacocha bulk ore and the low concentrations of Au found in Yerington bulk ore. However, the exposed high-sulfidation advanced argillic alteration zones in the volcanic rocks overlying the Yerington porphyry Cu deposits do not contain anomalous Au, and it appears unlikely that hydrothermal fluids at Yerington transported or deposited significant Au.

The magmatic sulfides at both Yerington and Yanacocha have Au/Cu ratios of about 10^{-4}, whereas ores from Yerington have a low average Au/Cu ~2 x 10^{-7} and

those from Yanacocha have a relatively high Au/Cu (estimated at 2 x 10^{-3}). Au/Cu fractionation is likely to occur both when magmatic sulfides are dissolved into magmatic hydrothermal fluids, and later when these hydrothermal fluids precipitate ore sulfides and gold. Additionally, metals may be contributed to the magmatic hydrothermal fluid from silicate melt as well as sulfide. The results of this study suggest that the copper, gold, and silver content and ratios of magmatic sulfides do not directly dictate the metal contents and ratios of related magmatic-hydrothermal ores. Further study is needed to test this hypothesis in the studied districts, and other localities.

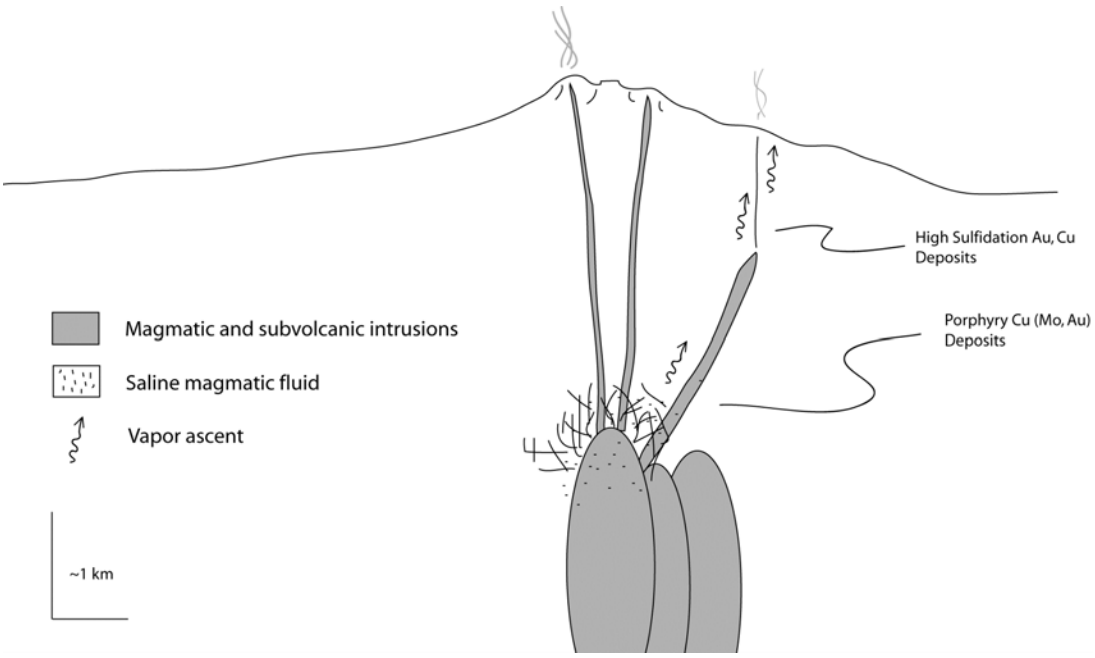

Figure 14 – Diagram modified from Hendenquist and Lowenstern (1994) showing the relationship of porphyry systems to that of high sulfidation systems above the source magma body.

Acknowledgements

This project was funded in part by NSF grant EAR-0337798 awarded to John Dilles of Oregon State University and Martin Streck of Portland State University. This funding, coupled with the direction, assistance, expertise from John Dilles, Adam Kent, Anthony Longo and other members of the Oregon State Geosciences Department made this project possible. The use of samples collected by John Dilles in the Yerington district and the Yanacocha samples collected by Anthony Longo was greatly appreciated. I would also like to thank the Newmont Mining Corporation for their financial and academic assistance during my three months spent in the summer of 2004 at the Yanacocha Mining Complex.

References

Barnes, H.; *Geochemistry of Hydrothermal Ore Deposits* (1979) John Wiley and Sons, Inc. p. 291-342

Bevington, P.; Data *Reduction and Error Analysis for the Physical Sciences* published by McGraw Hill (1969)

Buddington, A.; Lindsley, D.; Iron-Titanium Oxide minerals and synthetic equivalents. *Journal of Petrology* v. 5 (1964) p. 310-357

Dilles, J; The petrology and geochemistry of the Yerington Batholith and the Ann-Mason porphyry copper deposit, western Nevada. Doctoral Thesis, Stanford University (1984)

Dilles, J.; Wright, J.: The chronology of early Mesozoic arc magmatism in the Yerington District of western Nevada and its regional implications. *Geological Society of America Bulletin* v. 100 no. 5 (1986) p. 644-652

Dilles, J.; Petrology of the Yerington Batholith, Nevada: Evidence for Evolution of Porphyry Copper Ore Fluids. *Economic Geology* v. 82 (1987) p. 1750-1789

Dilles, J.; Proffett, J.; Metallogenesis of the Yerington Batholith, Nevada. Porphyry copper deposits of the American Cordillera *Arizona Geological Society Digest* v. 20 (1995) p. 306-315

Dilles, J.; Proffett, J.; Einaudi, M.; Barton, M.; Overview of the Yerington porphyry copper district; magmatic to nonmagmatic sources of hydrothermal fluids; their flow paths and alteration effects on rocks and Cu-Mo-Fe-Au ores. *Part I, Contrasting styles of intrusion-associated hydrothermal systems Guidebook Series - Society of Economic Geologists* v.32 (2000): p. 55-66

Eble, D.; Naldrett, A.; Crystallization of sulfide liquids and the interpretation of ore composition. *Canadian Journal of Earth Sciences* v. 34 (1997) p. 352-365

Halter, W.; Pettke, T., Heinrich, C.; The Origin of Cu/Au ratios in Porphyry-Type Ore Deposits. *Science* v. 296 issue 5574, (2002a) p.1844-1846

Halter, W.; Pettke, T.; Heinrich, C.; Major to Trace element analysis of melt inclusions by laser-ablation ICP-MS: methods of quantification. *Chemical Geology* 183 (2002b) p. 63-86

Halter, W.; Pettke, T.; Heinrich, C.; Laser Ablation ICP-MS analysis of silicate and sulfide melt inclusions in an andesitic complex I: analytical approach and data evaluation. *Contrib. Mineral Petrol* 147; (2004a) p. 385-396

Halter, W.; Pettke, T.; Heinrich, C.; Laser Ablation ICP-MS analysis of silicate and sulfide melt inclusions in an andesitic complex II: evidence for magma mixing and magma chamber evolution. *Contrib. Mineral Petrol* 147; (2004b) p. 397-412

Halter, W.; Heinrich, C.; Pettke, T.; Magma Evolution and the formation of porphyry Cu-Au or fluids: evidence from silicate and sulfide melt inclusions. *Mineralium Deposita* (2005) 39: p. 845-863

Harvey, B.; Myers, S.; Klein, T.; Yanacocha Gold District, Northern Peru. *Australasian Institute of Mining and Metallurgy* 4-99 (1999) p. 445-459

Hendenquist, J.; Lowenstern, J.; The role of magmas in the formation of hydrothermal ore deposits. *Nature* (1994) v. 370 p. 519-527

Hook, C.; Magmatic Sulfides in intermediate to mafic volcanic rocks contemporaneous with the ore-related plutonism at Bingham, Utah. Unpublished M.S. thesis, University of Georgia, Athens, Georgia. (1995)

Keith, J.; Whitney, J.; Hattori, K.; Ballantyne, E.; Christainsen, D.; Barr, D.; The Role of Magmatic Sulfides and Mafic Alkaline Magmas in the Bingham and Tintic Mining Districts, Utah. *Journal of Petrology* (1997) p. 1679-1690

Larocque, A.; Stimac, J.; Keith, J.; Evidence for open system behavior in immiscible Fe-S-O liquids in silicate magmas: implications for contributions of metals and sulfur to ore forming fluids *Canadian Mineralogist* v. 38 (2000) p. 1233-1249

Longerich, H.; Jackson, S.; Günther, D.; Laser ablation inductively coupled plasma mass spectrometric transient signal data acquisition and analyte concentration calculation *Journal of Analytical Atomic Spectrometry***,** (1996) p. 899 – 904

Longo, A.; The San Jose-Carachugo-Chaquicocha Gold Trend, Yanacocha District, Northern Peru. Unpublished document of the Newmont Mining Corporation (2000)

Longo, A.; Yanacocha Study – 2001 Field Season: Stratigraphy, Exploration Targets and Budget. Unpublished document of the Newmont Mining Corporation, December (2001)

Longo, A.; Saderholm, E.; Volcanic stratigraphy and host rocks of gold and copper ore in the Yanacocha mining district, Peru. Geological Society of America, Cordilleran Section, 98th annual meeting Abstracts with Programs - Geological Society of America
v. 34, (2002) no. 5

Longo, A.; Evolution of Volcanism and Hydrothermal Activity in the Yanacocha Mining District, Northern Peru. Oregon State University PhD Thesis (2005)

Naldrett, A.; Duke, M,; Lightfoot, P.; Thompson, J.; Quantitative Modeling of the segregation of magmatic sulfides: an exploration guide. *CIM Bulletin* v. 77 (1984) p. 46-56

Naney, M.; Phase equilibria of rock-forming ferromagnesian silicates in granitic systems. *American Journal of Science* (1983) Vol. 283, Issue 10, pp.993-1033

Stavast, W.; Keith, K.; Christiansen, E.; Dorais, M.; The Fate of Magmatic Sulfides During Intrusion or Eruption, Bingham and Tintic Districts, Utah. (2005) In press

Streck, M. and Dilles, J.; Sulfur evolution of oxidized arc magmas as recorded in apatite from a porphyry copper batholith *Geology*; (1998); v. 26; no. 6; p523-526

Sillitoe, R.; Gold deposits in western Pacific island arcs: the magmatic connection. Economic Geology Monograph v. 6 (1989) p. 274-291

Sillitoe, R.; Styles of High-Sulfidation gold, silver, and copper mineralization in porphyry and epithermal environments. *Australasian Institute of Mining and Metallurgy* 4-99 (1999) p. 29-44

Stimac, J.; Hickmott, D.; Ore metal partitioning in intermediate-to-silicic magmas: PIXE results on natural mineral/melt assemblages. In Clark, A. ed., *Giant ore deposits II: Controls on the scale of orogenic magmatic-hydrothermal mineralization: Proceedings of second giant ore deposits workshop, Kingston, Ontario, Canada, April 25-27*, (1995) p. 197-235

Stimac, J.; Pearce, T., Donnelly-Nolan, J.; The Origin and Implications of Undercooled Andesitic Inclusions in Rhyolites, Clear Lake Volcanics, California. *Journal of Geophysical Research*, v. 95, October (1990), No. B11, p 17729-17746

Stormer, J.; Whitney, J.; Two feldspar and iron-titanium oxide equilibria in silicic magmas and the depth of origin of large volume ash-flow tuffs. *American Mineralogist* (1985) p. 52-64

Turner, S.; The Yanacocha epithermal gold deposits, northern Peru; High sulfidation mineralization in a flow dome setting. PhD thesis, Colorado School of Mines (1997)

Turner, S.; Settings and styles of high-sulfidation gold deposits in the Cajamarca region, northern Peru. *Australasian Institute of Mining and Metallurgy* 4-99 (1999) p. 461-468

Whitney, J., Stormer, J.; Magmatic conditions and magma mixing in the Carpenter Ridge Tuff; a zoned ash-flow in the San Juan volcanic field, Colorado. *Eos Transactions, AGU* (1984) Vol. 65, Issue 45, pp. 1127

Wilson, S.; Ridley, W., Koenig, A.; Development of Sulfide calibration standards for the laser ablation inductively coupled plasma mass spectrometry technique *Journal of Analytical Atomic Spectrometry* V.17 (2002) p. 406-409

APPENDICES

Appendix Table 1 – Sample Locations and Occurrences

				Location - UTM (17M)	
Sample	**Mineral**	**Rock Unit**	**Host Mineral**	**Easting**	**Northing**
SJS-79A-01	Cp	SJI	Plag	775896	9225237
OCU-3-01	Py	Upha	Plag	Borehole	
YSBD-01	Py	Upha	Plag	774850	9226950
DN-7-01	Cp	MMI	Plag	774375	9230231
DN-7-03	Cp	MMI	Plag	774375	9230231
DN-7-04	Cb+Po?	MMI	Plag	774375	9230231
DN-30-01	Po	MMI	CPX	774882	9231674
DN-30-02	Po	MMI	Plag	774882	9231674
Exaltado-2	Po+Cb?	Lpha	Plag	766235	9221508
Exaltado-5	Cb+Po?	Lpha	Plag	766235	9221508
Exaltado-6	Cb	Lpha	Plag	766235	9221508
Exaltado-9	Po	Lpha	Plag	766235	9221508
Exaltado-10	Cp	Lpha	Plag	766235	9221508
Exaltado-11	Po	Lpha	Plag	766235	9221508
C Atazaico-01	Po	Lpha	OPX	762600	9218250
C Atazaico-02	ISS	Lpha	Plag	762600	9218250
C Atazaico-03	Po	Lpha	Plag	762600	9218250
C Atazaico-04	Po	Lpha	Plag	762600	9218250
C Atazaico-05	Cb?	Lpha	Plag	762600	9218250
C Atazaico-06	Po	Lpha	Plag	762600	9218250
C Atazaico-07	Po	Lpha	Plag	762600	9218250
C Atazaico-08	Cb?	Lpha	Plag	762600	9218250
C Atazaico-09	Cp	Lpha	Plag	762600	9218250
GP-4-01	Cb?	Lpha	Plag	759720	9226044
GP-4-02	Po+Cb?	Lpha	Plag	759720	9226044
GP-4-03	Cp	Lpha	Plag	759720	9226044
CA-1-01	Po	Lpha	Plag	758510	9218758
CA-1-02	Po	Lpha	Plag	758510	9218758
CR-3-01	Cp	Lpha	Plag	759616	9231040
CR-3-02	ISS	Lpha	Plag	759616	9231040
CR-3-03	Cp	Lpha	Plag	759616	9231040
DN-45-01	Po	BT	Plag	772790	9232830
DN-47-02	Py	BT	Plag	771931	9234501
DN-47-03	Po	BT	Plag	771931	9234501
Y-787-01	Cp	YB	K-spar	N/A	N/A
Y-787-02	Cp	YB	K-spar	N/A	N/A
Y-787-04	Cp	YB	K-spar	N/A	N/A
Y-790-01	Cp	YB	K-spar	N/A	N/A
Y-790-02	Cp	YB	K-spar	N/A	N/A
Y-790-03	Cp	YB	K-spar	N/A	N/A
Y-793-01	Cp	YB	K-spar	N/A	N/A
Y-793-02	Cp	YB	K-spar	N/A	N/A
Y-793-03	Cp	YB	K-spar	N/A	N/A

Chart showing the type of sulfide, rock unit, host mineral and UTM location where applicable.

Po – Pyrrhotite Py – Pyrite Cp – Chalcopyrite ISS – Intermediate Sulfide Solution
SJI – San Jose Ignimbrite Upha – Upper pyroxene hornblende andesite MMI – Maqui Maqui Ignimbrite
Lpha – Lower pyroxene hornblende andesite YB – Yerington Batholith
Plag – Plagioclase CPX – Clinopyroxene OPX – Orthopyroxene K-spar – Potassium Feldspar

Appendix Table 2 – Microprobe Data for All Magmatic Sulfides

Sample	SiO2	S	Fe	Cu	Wt % Total	Determined Mineral	Si	S	Fe	Cu	Atomic % Total
Yanacocha, Peru											
SJS-79A-01	26.0	25.4	18.3	22.9	92.7	**Cp**	22.8	41.6	17.3	19.0	100.6
OCU-3-01	2.1	53.7	47.3	0.3	103.4	**Py**	1.4	65.7	33.2	0.2	100.6
YSBD-1	73.2	10.8	6.5	0.0	90.4	**Py**	73.0	20.1	6.9	0.0	100.0
DN-7-03	52.0	2.3	1.8	2.4	58.5	**Cp**	86.0	7.1	3.3	3.7	100.1
DN-7-04	49.9	3.0	6.1	2.5	61.5	**Cb + Po?**	77.4	8.7	10.2	3.7	100.0
DN-30-01	0.2	40.2	62.6	0.3	103.4	**Po**	0.1	52.6	47.0	0.2	100.0
DN-30-02	9.5	33.4	52.1	2.9	98.0	**Po**	7.3	47.8	42.8	2.1	100.0
Exaltado - 02	18.8	24.4	32.8	12.0	88.0	**Po + Cb?**	16.9	41.2	31.7	10.2	100.0
Exaltado - 05	35.5	12.3	12.5	5.3	65.6	**Cb + Po?**	46.1	30.0	17.5	6.5	100.0
Exaltado - 08	45.3	6.7	5.7	4.9	62.6	**Cb**	66.1	18.3	8.9	6.8	100.1
Exaltado - 09	30.2	15.1	23.7	1.3	70.3	**Po**	35.4	33.2	29.9	1.4	100.0
Exaltado - 10	3.1	33.7	28.1	34.7	99.6	**Cp**	2.4	48.8	23.4	25.4	100.0
C Atatzaico-01	39.5	11.8	29.3	0.2	80.8	**Po**	43.3	24.3	34.5	0.2	102.3
C Atatzaico-05	43.5	6.9	8.4	4.5	63.3	**Cb?**	62.4	18.4	12.9	6.2	100.0
C Atatzaico-06	41.5	7.1	9.9	0.3	58.8	**Po**	63.1	20.2	16.2	0.5	100.0
C Atatzaico-07	0.0	22.2	35.0	0.2	57.5	**Po**	0.1	52.5	47.5	0.3	100.3
C Atatzaico-08	36.6	7.8	8.9	2.1	55.4	**Cb?**	58.3	23.2	15.3	3.2	100.0
GP-4-01	7.6	29.8	34.5	19.0	90.9	**Cb?**	6.4	47.1	31.3	15.2	100.0
GP-4-02	30.2	7.4	12.0	5.3	54.9	**Po + Cb?**	48.7	22.4	20.9	8.1	100.0
GP-4-03	6.7	26.0	21.6	26.9	81.3	**Cp**	6.5	46.8	22.3	24.4	100.0
CA-1-01	0.1	39.8	63.3	0.1	103.2	**Po**	0.1	52.3	47.7	0.0	100.0
CA-1-02	12.5	34.4	50.7	1.0	98.6	**Po**	9.4	48.7	41.2	0.7	100.0
CR-3-01	9.8	29.3	26.4	30.2	95.7	**Cp**	8.1	45.1	23.3	23.5	100.0
CR-3-02	24.0	21.5	22.8	21.3	89.7	**ISS**	22.0	37.0	22.5	18.5	100.0
DN-45-01	19.2	29.1	42.4	2.4	93.1	**Po**	15.8	44.8	37.5	1.9	100.0
DN-47-02	24.4	18.5	11.2	0.1	54.1	**Py**	34.3	48.6	16.9	0.1	100.0
DN-47-03	6.7	32.2	48.0	5.4	92.2	**Po**	5.4	48.7	41.8	4.2	100.0
Yerington, Nevada											
Y-787-01	32.5	24.0	18.5	20.4	95.4	**Cp**	27.6	38.3	16.9	16.4	100.0
Y-787-02	14.0	29.8	24.9	30.9	99.6	**Cp**	11.1	44.3	21.3	23.2	100.0
Y-787-03	18.1	27.4	22.7	28.4	96.6	**Cp**	14.9	42.5	20.2	22.2	100.0
Y-793-01	7.5	33.0	28.4	35.4	104.3	**Cp**	5.6	46.4	22.9	25.1	100.0

SiO_2 from the host silicate mineral is detectable in the sulfides due to the small size of the sulfide samples. Abbreviations found in Table 3.

Appendix Table 3 – Microprobe Standards and Intensities Used

	Standard Used	Peak	Intensity (cps / nA)
Si	KAUG_Mg_Si_Ca002	**Kα**	364.7
S	PYRI_S_Fe003	**Kα**	485.6
Fe	PYRI_S_Fe003	**Kα**	73.0
Cu	CHAL_Cu001	**Kα**	38.4

Electron Microprobe operating at 15 keV, 50 nA and a 1 μm beam diameter

Appendix Table 4 – Metal Ratios for Magmatic Sulfides from Each Rock Unit

	X10000	X10	X1000	X100
Unit Averages	**Au/Cu**	**Au/Ag**	**Ag/Cu**	**Pb/Cu**
San Jose Ignimbrite (11.3 Ma)	0.02	0.03	0.56	<DL
Upha (11.9 Ma)	<DL	<DL	10.9	123
Maqui Maqui Ignimbrite (12.5 Ma)	4.36	0.30	11.1	1.59
Lpha (14.2 Ma)	3.87	0.53	1.95	1.12
Biotite Tuff (15.4 Ma)	5.08	1.56	1.11	<DL
Yerington Batholith	1.23	1.58	1.60	2.52
Yanacocha	**3.96**	**0.50**	**3.38**	**8.82**
Yerington	**1.23**	**1.58**	**1.40**	**2.52**

Samples from Yanacocha are ordered by stratigraphy and age. Note the multiplication factor for each ratio.

Appendix Table 5 – Compositional Data for Iron Titanium Oxides from Yanacocha, Peru

CB-30	1	2	3	4	5	6	7	8	9	10	11	12	13
MgO	1.20	0.69	0.89	1.75	1.25	0.43	0.73	0.49	0.53	0.46	0.78	0.69	0.51
Al2O3	0.31	1.73	1.60	0.22	0.26	2.37	0.20	0.17	1.29	0.64	0.33	0.17	0.14
MnO	0.45	0.37	0.41	0.98	0.57	0.45	0.53	0.62	0.34	0.58	0.70	0.43	0.94
FeO	22.66	31.90	31.87	23.40	24.44	33.51	23.20	22.72	33.33	22.61	23.13	22.84	5.95
Fe2O3	47.67	61.39	60.56	42.67	43.86	55.32	46.15	47.03	57.74	48.02	45.10	47.56	59.55
ZnO	-0.01	0.25	0.19	0.06	0.10	0.26	0.07	0.01	0.21	0.09	0.00	0.11	0.21
SO2	-0.01	0.01	0.01	0.01	0.00	0.02	0.00	0.01	0.01	0.01	0.01	0.01	0.04
CaO	0.15	0.00	0.01	0.03	-0.01	0.11	0.05	0.02	0.08	0.02	0.09	0.05	4.04
TiO2	26.55	2.37	3.03	30.90	30.18	3.35	27.86	27.08	1.61	23.72	28.17	27.50	26.13
SiO2	0.02	0.14	0.07	0.06	0.04	1.14	0.04	0.09	2.24	2.38	0.16	0.09	0.23
Recalc Total	101.39	99.24	99.10	100.47	101.02	97.40	99.14	98.60	97.86	98.86	98.84	99.83	98.16
Fe2+	0.89	0.95	0.94	0.85	0.89	0.95	0.92	0.94	0.95	0.94	0.91	0.93	0.45
Fe3+	0.96	0.95	0.95	0.98	0.98	0.93	0.99	0.99	0.96	0.97	0.98	0.99	0.99
Xilm	0.53			0.57	0.57		0.54	0.53		0.50	0.54	0.53	0.31
Xusp		0.07	0.09			0.11			0.05				

Appendix Table 5 – Compositional Data (Continued)

COR-1	1	2	3	4	5	6	7	8	9	10	11	12	13
MgO	0.90	0.90	2.29	1.43	1.48	1.81	1.77	1.00	2.23	0.98	1.85	1.81	1.85
Cr2O3	0.09	0.03	-0.02	0.04	0.03	0.02	0.02	0.02	0.05	0.03	-0.02	0.03	-0.02
MnO	0.72	0.76	1.44	0.83	0.78	1.11	1.09	0.84	1.40	0.82	1.11	1.02	1.11
FeO	33.72	34.08	34.95	31.90	31.36	35.06	35.08	33.22	34.79	32.60	35.91	24.46	35.26
Fe2O3	57.27	56.84	21.68	30.41	31.11	23.28	24.06	57.06	22.33	54.99	22.56	31.47	23.44
ZnO	0.22	0.23	0.04	0.15	0.04	0.04	0.07	0.23	0.00	0.18	0.06	0.04	0.15
V2O3	0.44	0.42	0.28	0.31	0.30	0.25	0.20	0.43	0.25	0.42	0.25	0.25	0.21
TiO2	4.35	4.61	38.63	34.58	33.92	38.30	38.10	4.40	38.27	4.28	38.94	35.18	38.36
SiO2	0.05	0.04	0.03	0.03	0.04	0.05	0.00	0.04	0.03	0.10	0.05	0.10	0.01
Recalc Total	99.03	99.20	99.43	100.02	99.48	100.18	100.59	98.70	99.48	96.17	100.88	97.16	100.54
Fe2+	0.95	0.95	0.90	0.93	0.93	0.92	0.92	0.94	0.91	0.94	0.92	0.82	0.92
Fe3+	0.97	0.97	0.98	0.98	0.98	0.98	0.98	0.97	0.98	0.96	0.98	0.99	0.98
Xilm			0.79	0.71	0.70	0.78	0.77		0.78		0.79	0.67	0.78
Xusp	0.14	0.15						0.14		0.15			

COR-1	14	15	16	17	18	19	20	21	22	23	24	25	26
MgO	0.75	1.11	1.10	1.11	1.11	1.76	1.78	1.79	1.73	1.64	2.05	2.15	1.87
Cr2O3	0.00	0.01	0.04	0.06	0.01	-0.02	0.02	0.02	0.02	0.00	0.02	0.06	0.05
MnO	0.47	0.92	0.77	0.87	0.91	1.10	1.10	1.08	1.09	0.94	1.25	1.31	1.16
FeO	32.27	33.79	34.37	34.30	33.53	35.73	36.22	36.07	36.14	32.70	35.21	34.13	33.01
Fe2O3	56.53	58.11	57.67	57.29	53.75	22.23	22.26	22.18	22.20	28.86	21.40	22.41	25.62
ZnO	0.14	0.14	0.14	0.26	0.26	0.05	0.15	-0.04	0.11	0.13	0.17	0.07	0.04
V2O3	0.40	0.44	0.41	0.43	0.32	0.33	0.25	0.27	0.32	0.42	0.27	0.21	0.33
TiO2	3.00	4.64	4.83	4.79	4.81	38.67	39.18	39.05	39.10	35.51	38.74	37.64	35.98
SiO2	0.43	0.04	0.06	0.06	0.88	0.03	0.01	0.03	0.00	-0.01	0.03	0.05	0.01
Recalc Total	96.70	100.64	100.77	100.44	96.90	100.07	101.08	100.68	100.92	100.44	99.34	98.17	98.20
Fe2+	0.96	0.94	0.94	0.94	0.93	0.92	0.92	0.93	0.93	0.92	0.91	0.91	0.91
Fe3+	0.94	0.97	0.97	0.97	0.97	0.98	0.98	0.98	0.97	0.98	0.98	0.98	0.98
Xilm						0.79	0.79	0.79	0.79	0.72	0.79	0.78	0.75
Xusp	0.11	0.15	0.15	0.15	0.16								

COR-1	27	28	29
MgO	1.12	1.02	1.07
Cr2O3	0.01	0.03	0.01
MnO	0.89	0.86	0.82
FeO	33.08	33.69	33.30
Fe2O3	54.51	57.04	57.02
ZnO	0.20	0.24	0.24
V2O3	0.45	0.47	0.42
TiO2	4.63	4.60	4.40
SiO2	0.20	0.02	0.07
Recalc Total	96.48	99.27	98.58
Fe2+	0.94	0.94	0.94
Fe3+	0.96	0.97	0.97
Xilm			
Xusp	0.16	0.15	0.14

Appendix Table 5 – Compositional Data (Continued)

CR-3	1	2	3	4	5	6	7	8	9	10	11	12	13
MgO	3.42	3.26	2.33	2.22	3.19	2.51	6.84	1.31	2.49	2.37	1.43	2.06	2.07
Al2O3	4.13	3.07	3.49	3.34	3.32	3.50	0.16	1.33	0.09	1.08	1.34	2.68	2.55
MnO	0.73	0.61	0.41	0.49	0.59	0.44	0.90	0.51	0.72	1.32	0.55	0.41	0.47
FeO	37.57	36.10	32.37	32.80	36.47	33.95	40.87	35.25	8.44	7.41	34.73	34.05	35.30
Fe2O3	35.73	43.64	53.86	48.73	42.69	50.34	2.07	51.95	34.40	73.08	47.51	49.59	50.14
ZnO	0.36	0.11	0.15	0.10	0.14	0.15	0.00	0.18	0.06	0.01	0.25	0.14	0.13
V2O3	0.34	0.35	0.45	0.39	0.37	0.46	0.22	0.56	0.18	0.45	0.45	0.57	0.58
TiO2	8.98	9.70	4.88	5.57	10.02	6.22	49.43	6.30	36.81	11.37	7.57	6.36	6.54
SiO2	4.66	0.07	0.06	0.68	0.10	0.37	0.02	0.49	0.13	0.07	0.06	0.06	0.63
Recalc Total	96.30	97.18	98.31	94.47	97.16	98.12	100.76	98.09	91.74	97.29	94.08	96.04	98.57
Fe2+	0.83	0.90	0.91	0.92	0.90	0.91	0.84	0.94	0.42	0.67	0.94	0.93	0.93
Fe3+	0.84	0.92	0.92	0.92	0.91	0.92	0.84	0.96	0.99	0.98	0.96	0.93	0.93
Xilm							0.98		0.53	0.22			
Xusp	0.33	0.33	0.17	0.20	0.34	0.21		0.21			0.26	0.22	0.22

CR-3	13	14	15	16	17	18	19	20	21	22	23	24	25	26
MgO	2.07	4.28	1.62	1.89	2.04	1.57	1.32	1.36	4.81	1.40	1.38	1.39	1.32	2.52
Al2O3	2.55	0.21	2.71	2.71	2.54	1.50	1.37	1.31	0.18	1.33	1.47	1.37	1.31	2.58
MnO	0.47	0.67	0.43	0.40	0.48	0.60	0.51	0.53	3.15	0.60	0.55	0.65	0.54	0.52
FeO	35.30	39.37	35.26	33.96	34.98	37.22	34.89	34.85	39.63	35.63	34.30	36.57	27.82	36.02
Fe2O3	50.14	8.25	51.62	49.85	51.29	44.15	52.47	52.44	1.81	50.75	51.01	49.56	54.96	50.54
ZnO	0.13	-0.04	0.21	0.18	0.11	0.09	0.09	0.19	0.00	0.15	0.20	0.21	0.18	0.21
V2O3	0.58	0.22	0.62	0.56	0.55	0.43	0.52	0.48	0.21	0.46	0.51	0.57	0.46	0.48
TiO2	6.54	44.61	6.04	5.88	6.46	8.99	6.15	6.49	47.85	7.41	6.28	7.76	7.02	7.59
SiO2	0.63	0.03	0.40	0.09	0.09	0.38	0.06	0.05	0.07	0.36	0.10	0.18	0.38	0.04
Recalc Total	98.57	97.68	99.04	95.55	98.66	95.01	97.40	97.85	97.82	98.53	95.89	98.41	96.64	100.60
Fe2+	0.93	0.89	0.94	0.93	0.93	0.94	0.95	0.94	0.83	0.94	0.94	0.94	0.86	0.92
Fe3+	0.93	0.95	0.93	0.93	0.94	0.95	0.96	0.96	0.81	0.96	0.96	0.96	0.97	0.94
Xilm		0.92							0.98					
Xusp	0.22		0.21	0.21	0.22	0.31	0.20	0.21		0.24	0.21	0.25	0.20	0.25

CR-3	27	28	29	30	31	32	33	34	35	36	37
MgO	2.47	2.53	2.22	4.90	2.41	2.53	2.34	4.89	2.45	1.72	1.65
Al2O3	2.53	2.72	2.73	0.19	2.69	2.69	2.70	0.17	2.60	1.30	1.33
MnO	0.53	0.51	0.48	0.74	0.50	0.57	0.50	0.86	0.59	0.42	0.64
FeO	35.43	36.00	35.14	40.42	36.48	36.21	35.53	40.32	36.26	32.72	37.95
Fe2O3	48.43	47.55	47.33	7.79	47.05	47.61	48.12	5.34	47.16	55.34	46.55
ZnO	0.10	0.18	0.13	0.07	0.18	0.17	0.15	-0.06	0.08	0.15	0.17
V2O3	0.46	0.52	0.56	0.28	0.54	0.45	0.49	0.13	0.45	0.49	0.50
TiO2	7.72	7.98	7.29	46.28	8.38	8.23	7.35	46.64	8.21	4.75	8.92
SiO2	0.06	0.19	0.16	0.00	0.12	0.09	0.53	0.03	0.26	0.08	0.35
Recalc Total	97.89	98.27	96.10	100.75	98.46	98.68	97.90	98.54	98.26	97.15	98.08
Fe2+	0.92	0.92	0.93	0.87	0.92	0.92	0.92	0.87	0.92	0.93	0.94
Fe3+	0.93	0.93	0.93	0.93	0.93	0.93	0.93	0.94	0.93	0.96	0.96
Xilm				0.93				0.95			
Xusp	0.26	0.27	0.25		0.28	0.27	0.25		0.28	0.16	0.29

Appendix Table 5 – Compositional Data (Continued)

DN-53	1	2	3	4	5	6	7	8	9	10	11	12	13
MgO	1.77	2.68	1.51	0.96	2.67	1.52	0.85	1.28	3.47	1.20	2.25	2.74	0.47
Al2O3	1.75	1.86	2.10	0.13	0.12	1.26	1.36	1.68	0.12	1.74	0.14	0.18	1.54
MnO	0.40	0.65	0.45	3.42	2.82	0.48	0.36	0.64	1.86	0.62	2.10	0.55	0.14
FeO	29.93	32.05	31.12	35.79	37.35	33.61	35.45	32.92	38.36	32.15	37.86	34.47	32.75
Fe2O3	63.68	58.24	62.05	19.04	15.28	58.53	54.50	57.58	11.82	59.35	14.71	23.62	62.23
ZnO	0.09	0.19	0.22	0.06	-0.04	0.21	0.20	0.24	0.05	0.17	0.01	0.14	0.16
V2O3	0.43	0.34	0.39	0.22	0.20	0.38	0.42	0.53	0.24	0.46	0.24	0.34	0.47
TiO2	1.60	4.13	2.20	40.64	43.03	4.32	5.18	4.00	44.15	3.38	42.48	37.98	2.22
SiO2	0.04	0.04	0.05	0.04	0.04	0.06	0.77	0.06	0.04	0.02	0.04	0.01	0.13
Recalc Total	99.91	100.28	100.17	100.43	101.59	100.43	99.27	99.00	100.27	99.23	99.97	100.05	100.17
Fe2+	0.92	0.90	0.93	0.89	0.87	0.94	0.96	0.94	0.87	0.94	0.90	0.91	0.98
Fe3+	0.96	0.96	0.96	0.98	0.98	0.97	0.96	0.96	0.97	0.96	0.97	0.98	0.97
Xilm				0.82	0.85				0.89		0.86	0.77	
Xusp	0.05	0.13	0.07			0.14	0.17	0.13		0.11			0.07

DN-53	14	15	16	17	18	19	20	21	22	23	24	25	26
MgO	2.57	0.32	1.21	1.83	2.32	2.12	1.38	2.88	1.31	1.38	4.28	1.34	2.50
Al2O3	0.16	0.96	0.18	2.09	2.28	0.45	1.88	0.50	1.95	1.38	0.13	1.45	0.13
MnO	1.05	0.12	1.83	0.36	0.49	0.31	0.42	2.15	0.46	0.57	1.66	0.48	2.50
FeO	34.36	33.35	32.17	31.73	31.36	20.70	33.33	31.53	33.00	31.16	35.86	31.95	34.70
Fe2O3	23.05	60.81	28.00	59.69	58.15	51.41	58.02	24.68	57.36	60.97	15.99	60.82	18.89
ZnO	0.00	0.10	0.01	0.24	0.12	-0.07	0.13	0.18	0.17	0.19	0.11	0.18	0.08
V2O3	0.30	0.49	0.38	0.52	0.42	0.29	0.48	0.23	0.40	0.51	0.30	0.50	0.23
TiO2	38.08	2.52	35.46	3.13	3.94	23.90	4.02	36.81	3.84	2.55	42.09	2.83	40.42
SiO2	0.02	0.57	0.00	0.04	0.06	0.03	0.06	0.05	0.05	0.06	0.03	0.05	0.05
Recalc Total	99.62	99.38	99.36	99.74	99.46	99.46	99.80	99.06	98.52	98.88	100.48	99.65	99.72
Fe2+	0.90	0.98	0.91	0.93	0.91	0.89	0.95	0.86	0.94	0.94	0.86	0.94	0.87
Fe3+	0.98	0.97	0.98	0.95	0.95	0.98	0.96	0.97	0.96	0.97	0.97	0.97	0.98
Xilm	0.78		0.73			0.49		0.75			0.84		0.82
Xusp		0.09		0.10	0.13		0.13		0.13	0.08		0.09	

DN-53	27	28	29	30	31	32	33	34	35	36	37
MgO	1.40	1.10	0.82	2.86	0.61	0.41	1.73	2.48	0.38	2.40	1.25
Al2O3	1.36	0.47	1.59	0.18	1.53	1.56	0.65	0.13	1.01	0.17	0.54
MnO	0.66	0.37	0.52	1.67	0.39	0.27	0.89	0.67	0.13	0.73	0.78
FeO	34.05	25.69	31.13	32.67	31.71	33.94	28.82	33.96	33.62	33.04	19.44
Fe2O3	54.36	43.30	60.76	23.50	61.32	56.94	37.16	24.95	62.42	26.66	51.79
ZnO	0.10	0.07	0.20	0.15	0.15	1.18	0.02	0.05	0.11	0.04	0.11
V2O3	0.28	0.40	0.29	0.25	0.52	0.41	0.27	0.35	0.49	0.34	0.33
TiO2	5.59	27.20	2.12	37.52	1.98	4.49	31.25	37.43	2.67	36.43	21.16
SiO2	0.05	0.06	0.16	0.04	0.06	0.08	0.33	0.03	0.05	0.02	0.69
Recalc Total	97.94	98.70	97.61	98.91	98.24	99.29	101.18	100.19	100.90	99.86	96.20
Fe2+	0.94	0.94	0.95	0.87	0.96	0.95	0.91	0.91	0.98	0.91	0.90
Fe3+	0.97	0.98	0.97	0.98	0.96	0.96	0.97	0.98	0.97	0.98	0.98
Xilm		0.58		0.77			0.64	0.76		0.74	0.47
Xusp	0.18		0.07		0.07	0.15			0.09		

Appendix Table 5 – Compositional Data (Continued)

DN-7	1	2	3	4	5	6	7	8	9	10	11	12	13
MgO	0.96	1.31	0.99	1.85	1.86	1.77	1.81	1.35	1.61	1.59	1.64	1.75	1.85
Al2O3	0.36	1.24	2.70	0.22	0.23	0.22	0.93	1.71	1.77	1.74	1.42	1.41	0.25
MnO	0.74	0.84	0.28	0.55	0.55	0.51	0.70	0.50	0.59	0.58	0.54	0.63	0.34
FeO	25.93	29.52	25.91	30.09	30.39	29.84	30.24	31.90	31.64	31.92	30.25	30.37	24.83
Fe2O3	39.94	62.33	24.38	34.41	33.14	35.73	59.71	62.40	60.10	59.49	63.81	63.01	44.97
ZnO	0.13	0.20	0.07	0.13	0.04	-0.01	0.06	0.15	0.33	0.13	0.20	0.24	0.00
V2O3	0.28	0.36	0.34	0.37	0.32	0.34	0.35	0.44	0.42	0.42	0.45	0.40	0.36
TiO2	28.38	1.58	21.76	32.70	32.90	31.94	3.08	2.24	3.00	3.34	1.42	2.32	26.64
SiO2	0.85	0.16	6.78	0.04	0.03	0.08	0.70	0.08	0.08	0.06	0.08	0.06	0.35
Recalc Total	98.08	97.69	83.61	100.42	99.57	100.40	98.19	100.80	99.62	99.39	99.87	100.46	99.61
Fe2+	0.92	0.92	0.94	0.92	0.93	0.93	0.91	0.94	0.93	0.93	0.93	0.91	0.92
Fe3+	0.98	0.97	0.88	0.98	0.98	0.98	0.98	0.96	0.96	0.96	0.97	0.97	0.98
Xilm	0.60		0.68	0.67	0.68	0.66							0.56
Xusp		0.05					0.10	0.07	0.10	0.11	0.05	0.07	

DN-7	14	15	16	17	18	19	20	21
MgO	1.75	1.66	1.76	1.92	1.71	1.59	1.77	1.62
Al2O3	0.28	0.27	0.25	0.24	0.18	0.21	0.22	0.21
MnO	0.34	0.33	0.36	0.35	0.38	0.33	0.32	0.34
FeO	23.86	24.22	25.95	25.36	24.39	25.80	25.33	26.69
Fe2O3	47.17	47.16	45.13	45.02	46.40	45.03	44.91	43.02
ZnO	0.10	-0.05	0.02	0.06	0.08	-0.01	0.05	0.04
V2O3	0.34	0.37	0.38	0.36	0.34	0.35	0.37	0.46
TiO2	25.68	26.49	28.16	28.02	26.87	28.02	27.59	28.70
SiO2	0.37	0.03	0.02	0.03	0.05	0.05	0.03	0.02
Recalc Total	99.87	100.59	102.05	101.52	100.56	101.48	100.68	101.11
Fe2+	0.92	0.92	0.92	0.91	0.92	0.93	0.92	0.93
Fe3+	0.99	0.99	0.98	0.98	0.99	0.99	0.98	0.98
Xilm	0.54	0.54	0.57	0.57	0.55	0.57	0.57	0.59
Xusp								

Appendix Table 5 – Compositional Data (Continued)

DN-30	1	2	3	4	5	6	7	8	9	10	11	12	13
MgO	1.81	1.08	1.10	0.41	1.02	1.19	1.83	1.85	0.79	1.42	0.85	1.07	0.78
Al2O3	1.28	1.80	1.78	0.80	1.78	1.95	0.18	0.17	1.52	0.17	1.48	1.99	1.31
MnO	0.78	0.46	0.40	0.14	0.37	0.49	0.53	0.56	0.40	0.52	0.41	0.40	0.33
FeO	9.32	33.40	33.51	37.74	32.91	33.64	31.32	31.29	33.00	31.33	33.37	34.11	32.74
Fe2O3	74.79	58.42	58.66	47.46	59.37	58.39	28.90	29.62	61.38	29.91	60.14	57.81	57.43
ZnO	0.06	0.15	0.09	0.11	0.13	0.12	0.00	0.05	0.19	0.07	0.18	0.17	0.21
V2O3	0.42	0.40	0.42	0.42	0.45	0.40	0.30	0.31	0.52	0.32	0.51	0.42	0.47
TiO2	14.96	4.61	4.40	7.81	3.69	4.82	38.95	39.40	3.35	38.32	4.09	4.91	4.10
SiO2	0.07	0.08	0.03	1.40	0.27	0.07	0.03	0.02	0.05	0.03	0.05	0.05	0.11
Recalc Total	103.59	100.50	100.43	96.41	100.06	101.11	102.02	103.36	101.25	102.16	101.17	100.97	97.52
Fe2+	0.70	0.93	0.93	0.97	0.93	0.92	0.89	0.89	0.94	0.91	0.94	0.93	0.95
Fe3+	0.97	0.95	0.95	0.97	0.95	0.94	0.98	0.98	0.95	0.98	0.95	0.94	0.96
Xilm	0.25						0.72	0.71		0.71			
Xusp		0.13	0.13	0.25	0.11	0.14			0.10		0.12	0.14	0.12

DN-30	14	15	16	17	18	19	20	21
MgO	1.05	1.12	1.92	1.02	2.26	0.97	0.80	0.82
Al2O3	1.79	1.92	0.21	1.62	0.20	1.79	1.76	1.67
MnO	0.45	0.52	0.53	0.33	0.73	0.43	0.36	0.33
FeO	33.69	34.16	31.94	36.23	31.05	33.22	32.38	32.37
Fe2O3	58.78	56.88	27.09	56.04	28.03	59.78	62.64	62.38
ZnO	0.14	0.08	0.07	0.12	0.06	0.18	0.24	0.07
V2O3	0.43	0.40	0.30	0.53	0.28	0.51	0.51	0.48
TiO2	4.57	5.49	39.98	6.62	39.64	3.88	2.49	2.56
SiO2	0.05	0.06	0.00	0.06	0.01	0.08	0.05	0.03
Recalc Total	101.07	100.77	102.05	102.68	102.20	100.86	101.24	100.73
Fe2+	0.93	0.93	0.89	0.94	0.87	0.93	0.94	0.95
Fe3+	0.95	0.94	0.98	0.95	0.98	0.95	0.95	0.95
Xilm			0.74		0.73			
Xusp	0.13	0.16		0.19		0.11	0.07	0.08

Appendix Table 5 – Compositional Data (Continued)

SJS-79A 20.3m	1	2	3	4	5	6	7	8	9	10	11	12	13
MgO	1.98	1.01	1.82	1.82	1.51	1.76	1.65	1.90	1.95	1.85	1.86	1.95	2.18
Al2O3	8.98	1.08	0.13	0.14	0.11	0.14	0.16	0.18	0.14	0.14	0.14	0.16	0.11
MnO	0.53	0.34	0.54	0.58	0.45	0.44	0.40	0.45	0.55	0.54	0.58	0.63	0.84
FeO	33.86	31.97	28.03	28.45	26.13	26.99	25.82	26.77	28.92	25.80	26.60	26.45	28.43
Fe2O3	39.74	62.58	36.13	34.79	39.88	38.40	41.52	37.31	32.49	39.27	37.65	38.85	32.48
ZnO	0.22	0.17	0.01	0.15	0.05	0.02	0.07	0.01	0.03	-0.02	0.02	0.06	0.06
V2O3	0.37	0.52	0.34	0.35	0.27	0.31	0.39	0.34	0.37	0.34	0.41	0.39	0.34
TiO2	2.90	2.77	35.35	35.95	32.77	34.23	32.50	34.24	36.75	33.06	34.13	34.28	36.92
SiO2	4.23	0.08	0.02	0.04	0.04	0.01	0.02	0.06	0.05	0.02	0.04	0.03	0.05
Recalc Total	93.20	100.55	102.36	102.24	101.29	102.36	102.58	101.34	101.31	101.10	101.56	102.93	101.43
Fe2+	0.88	0.93	0.88	0.88	0.89	0.88	0.88	0.87	0.88	0.87	0.87	0.86	0.86
Fe3+	0.73	0.97	0.98	0.98	0.99	0.99	0.98	0.98	0.98	0.98	0.98	0.98	0.98
Xilm			0.65	0.66	0.61	0.63	0.60	0.63	0.68	0.61	0.63	0.62	0.68
Xusp	0.15	0.08											

SJS-79A 20.3m	14	15	16	17	18
MgO	0.90	1.08	0.99	1.14	1.09
Al2O3	0.82	1.13	1.09	1.13	1.15
MnO	0.31	0.34	0.29	0.43	0.43
FeO	31.31	31.14	31.13	32.06	30.79
Fe2O3	63.94	62.86	63.00	61.16	61.58
ZnO	0.09	0.15	0.27	0.20	0.19
V2O3	0.52	0.54	0.55	0.47	0.51
TiO2	2.11	2.26	2.25	3.50	3.11
SiO2	0.06	0.10	0.06	0.06	0.23
Recalc Total	100.15	99.66	99.67	100.24	99.43
Fe2+	0.94	0.93	0.93	0.92	0.91
Fe3+	0.97	0.96	0.96	0.96	0.96
Xilm					
Xusp	0.06	0.06	0.06	0.10	0.09

Electron microprobe data of the seven samples from Matthew Harper (2005, written communication) used to determine the temperature and oxygen fugacity of the Yanacocha samples. The method of Stormer and Whitney (1985) was used for the recalculation of oxides. OSU SX-100 electron microprobe used for analyses, using natural and synthetic standards.